Chapter 16

Automated Event and Phase Identification

(Version August 2011; DOI: 10.2312/GFZ.NMSOP-2_ch16)

Ludger Küperkoch [1)], Thomas Meier [2)], and Tobias Diehl [3)]

[1)] Ruhr-Universität Bochum, Institut für Geologie, Mineralogie und Geophysik, Universitätsstr. 150, 44780 Bochum
Now at: BESTEC GmbH, Oskar-von-Miller-Str. 2, 76829 Landau, E-mail: kueperkoch@bestec-for-nature.com

[2)] Universität Kiel, Institut für Geophysik, Otto-Hahn-Platz 1, 24118 Kiel, Fax: +49 431 880-4432, E-mail: meier@geophysik.uni-kiel

[3)] Swiss Seismological Service, ETH Zurich, Sonneggstrasse 5, 8092 Zürich, Switzerland, E-mail: tobias.diehl@sed.ethz.ch

Introduction

In Chapters 2 and 11 the complexity of seismic waveforms is explained in detail. Much experience is needed to identify the seismic phases correctly and to pick onset times accurately and consistently. The majority of our current knowledge of the Earth's seismicity

is based on manual picking of onset times. In addition, manual picks have been used for the investigation of the structure of the Earth. However, for early warning purposes and for the processing of large data sets automatic picking is needed. Because of the variability of seismic waveforms, the occurrence of different seismic phases and the presence of noise, automatic picking remains still a challenge. Yet, in the light of the rapidly growing amount of digital waveform data produced by permanent and temporary networks, the issue of automatic event detection and phase picking becomes more and more important. Accordingly, the number of published algorithms has increased significantly during the past years. This makes it difficult for potential users to keep track of the different approaches and developments, even more, since most algorithms have been developed for a certain data set or a particular problem, such as early warning, real-time location, tomography, etc. Accordingly, only few algorithms were widely established in the community of observational seismology. Generalization of essential principles and criteria as well as large-scale comparative benchmark tests of different existing algorithms are still extremely rare. This makes it difficult for interested developers to choose the most appropriate approach, especially when aiming at multi-task high-quality performance, and for users to select the most suitable algorithms among the many available techniques for their specific problem. With this Chapter we intend, therefore, to provide a broader introduction into the problem of automated event detection and phase identification, to outline the underlying theory and methodological approaches, to illustrate results produced by different procedures, to assess the performance of available algorithms, to sketch the likely development in the near future and to highlight essential practical considerations for the application of automatic picking procedures.

16.1.1 General Remarks

With the advent of digital real-time acquisition systems automated real-time event detection and location became feasible. Beginning around 1975, High Gain Long Period (HGLP) stations, including both digital and optical recordings, were deployed by the Seismic Research Observatories (SRO). WWSSN-stations were digitally upgraded (DWWSN), which constitute the Global Digital Seismic Network (GDSN) (e.g. Lay and Wallace, 1995). At the same time, rapid advances in computer technology enabled sophisticated analysis of increasing amount of seismic data. Nowadays, several digital, global seismic networks are in operation, monitoring continuously the global seismicity and providing rapid locations of earthquakes within minutes. Automated rapid and robust detection and location of earthquakes using real-time data of regional and global networks is essential for earthquake early warning systems. Usually, only automated first onset picks are used. A large number of automated P picks is required to ensure the robustness of the automated location. Fast automated locations are replaced after some time by more accurate manual locations that use also picks of later phases.

The need for automatic picking algorithms arises also from the increasing amount of digital data sets produced by modern passive seismic networks. Even local, temporary networks, as needed for reservoir characterization during stimulation experiments at enhanced geothermal systems (EGS) or hydrocarbon reservoirs, monitor ten-thousands of seismic events at high sampling rates. For tomographic studies, which usually require data merged from several seismological networks, highly accurate and consistent phase arrival times are needed. Automated post-processing algorithms have been developed to determine and select consistently high-quality picks for tomographic purposes whose quality might be even better than those of manual phase readings. The examples given above are typical applications of

automated seismic event detection and automated arrival time estimation. Automated processing schemes show the following potentials:

- fast and near-real time data processing;
- consistent arrival time estimation;
- processing of large data sets;
- if implemented, consistent onset quality estimation and phase identification.

The algorithms to choose depend on the specific application. Of course, the more precise and powerful the automated onset determination is, the more computationally expensive the applied algorithms are. For rapid earthquake location estimates or phase identification simple STA/LTA detections may be sufficient. E.g., Earle and Shearer (1994) use STA/LTA ratios taken from a smoothed envelope function, determined using a Hilbert transformation of the seismogram, to detect first and later arrivals. These algorithms are usually referred to as *phase detectors* in contrast to more accurate arrival time estimation algorithms, which are usually referred to as *phase pickers* (Baer and Kradolfer, 1987) and needed for precise location of earthquakes or tomographic studies. There is a considerable amount of automated picking algorithms available. Usually, these algorithms are optimized for certain requirements. Comparative studies and calibration tests are not yet common practice. While the STA/LTA detector is described in detail in Information Sheet IS 8.1, we here review the most widespread automatic picking algorithms and analyze their properties. An introduction to automatic phase identification is given.

Also the accuracy of manual readings is limited due to sampling rate, noise, or the occurrence of emergent onsets. These uncertainties must be added to the theoretical time resolution of modern, GPS-based broadband seismic networks, which allow precisions of P-onset readings within 0.2 s (e.g.; iP phases in teleseismic events; Leonard, 2000). Further problems are the inconsistency of manual picks, phase misidentification and incomplete documentation of applied filters. Douglas et al. (1997) compared P-wave readings of explosion and earthquake recordings. He showed that errors of manual picks are in the order of 0.1 seconds for explosions and about 0.5 seconds for teleseismic earthquakes with a magnitude range from 4.6 to 6.1. Using data of the Montana Bureau of Mines and Geology (MBMG) network, Zeiler and Velasco (2009) investigated manual picks of local and regional first arrivals. They found that the pick error is 0.1 seconds for phase measurements with high signal-to-noise ratios. Furthermore, the manual readings were biased towards late picks. Interestingly, in a second study using data collected by the International Seismological Center (ISC), they found that picks by different institutions may be inconsistent though individual institutions pick consistently. The standard deviation from the average arrival time determined from readings of several institutions for one single event varied between 0.2-0.6 seconds. For location purposes, the pick uncertainty should be significantly lower than the RMS-travel time residuals due to wave propagation effects not accounted for. From this point of view it is obvious that automatic phase picking has the potential to improve the consistency of arrival time estimations if it is supplemented by thorough quality estimations.

In the entire processing scheme from automated event detection to automated event location, usually a phase detector is applied to all available recordings first. Then the consistency of these detections is checked in order to detect an event. After a seismic event has been recognized, the more precise phase picker is applied to the time series to obtain arrival time estimations for a robust earthquake location. Following this basic processing scheme, section

16.2 gives an introduction to event detection based on phase detectors applied to a network of stations. In section 16.3 the following established P-phase picking algorithms are described: (1) the Allen-picker, (2) the Baer- and Kradolfer-picker, (3) picking based on Higher Order Statistics (HOS) and (4) Autoregressive-Akaike-Information-Criterion-picker (AR-AIC). Picking of later arrivals is briefly introduced in section 16.4. Automated algorithms for quality estimation and phase identification as well as outlier detection are discussed in section 16.5. Practical considerations on automatic picking, pre-processing and calibration are given in section 16.6.

The following section gives a brief overview on existing phase detection and picking algorithms. As the algorithms are presented in chronological order, this sub-section serves as a short historical overview on the development of automated picking algorithms.

16.1.2 Historical overview

One of the first mathematically based signal detectors was the one proposed by Freiberger (1963), who applied an approximate comparison of spectral densities for the detection of Gaussian signals in Gaussian noise. This method is suitable for detecting signals rather than measuring signal onset times. Stewart (1977) developed an automated procedure for P-phase detection, P-phase processing and coda processing for local seismic event analysis in central California. Using three moving windows for computing "moving-time noise averages" from the original seismic trace and its first difference, it is tested, whether the seismic station is operating within acceptable limits of noise or not. A P phase is detected, if the threshold exceeds 2.9 times the noise level. Goforth and Herrin (1981) developed an automatic seismic signal detector based on the Walsh transform, which is quite similar to the Fourier transform but computationally less expensive. Michael et al. (1982) used this approach to develop a real-time event detection and recording system for the MIT Seismic Network. Joswig (1987) proposed a pattern recognition technique using characteristic event features in spectrograms. However, the precision of these algorithms is limited.

A fundamental step towards automatic phase-onset determination was the algorithm proposed by Rex V. Allen (1978, 1982). He introduced the concept of the characteristic function (CF), resulting from non-linear transformations of the seismic trace to which a picker is applied. Allen's CF is based on short-term-average to long-term-average ratios (STA/LTA) calculated from an approximative squared envelope function of the seismogram. This picking algorithm is still frequently applied and used for automatic picking e.g by the USGS Earthworm system (Johnson et al., 1995). Baer and Kradolfer (1987) developed an automatic phase picker by slightly changing Allen's envelope function and incorporating a dynamic signal threshold. This algorithm marks a milestone in automated phase picking and is still frequently used, e.g. in the Programmable Interactive Toolbox for Seismological Analysis (PITSA, Scherbaum and Johnson, 1992) and MannekenPix (Aldersons, 2004). Furthermore, in combination with a sophisticated quality assessment this algorithm yields high-quality onset times useful for tomographic studies (e.g. Di Stefano et al., 2006, Diehl et al., 2009b). Higher order statistics are proposed e.g. by Saragiotis et al. (2002) and Küperkoch et al. (2010) where skewness and kurtosis are calculated in sliding windows generating the CF. These algorithms provide very reliable P-arrival time estimates.

Beside these time and frequency domain approaches, model oriented algorithms became quite common, too. Autoregressive (AR) techniques are widely used. Based on the Akaike

Information Criterion (AIC), Takanami and Kitagawa (1988) developed a procedure for the fitting of a locally stationary autoregressive model to seismograms. They implemented this procedure in an on-line system and called it FUNIMAR (fast univariate case of minimum AIC method of AR model fitting). Leonard and Kennett (1999) propose an autoregressive method that detects increases in the AR-model order due to the higher complexity of signals compared to preceding noise. The standard autoregressive two-model Akaike Information Criterium (AR-AIC, e.g. Sleeman and van Eck, 1999) estimates the AR coefficients from predefined noise and signal windows.

Gentili and Michelini (2006) propose an artificial neural network approach for P- and S-phase onset time determination, called innovative model of neural network (IUANT2). They use variance, skewness, kurtosis and a combination of skewness and kurtosis and their time derivatives.

Many automatic phase-detection algorithms incorporate several approaches, using the different advantages of the applied methods (e.g. Zhang et al., 2003; Bai and Kennett, 2000). Nippress et al. (2010) applied STA/LTA picker, higher order statistics (Saragiotis et al. 2002) and damped predominant period T^{pd} (Hildyard et al., 2008; Hildyard and Rietbrock, 2010) picker to ANCORP data to estimate P- as well as S-arrival times.

Algorithms for the estimation of relative travel times instead of absolute ones have been proposed in order to improve the picking accuracy. Examples are multi-station and array approaches using cross-correlation methods (VanDecar and Crosson, 1990) or adaptive stacking techniques (e.g. Rawlinson and Kennett, 2004; Rowe et al., 2002). These methods require high waveform coherence at neighboring stations and high signal to noise ratios as is observed for example in the case of low-pass filtered teleseismic waveforms.

16.2 Phase and event detection

In order to obtain first rough P-phase arrival time estimates, a single-station detector - e.g. a simple STA/LTA trigger (see IS 8.1) - is applied to all available continuous data streams of a seismic network. An analog or digital version of this detector might be implemented directly at the stations. Then data in a short time interval following the detection are transmitted to the data center for further analysis. Nowadays, usually continuous data streams are transferred to the data centers where a phase detector is applied to the incoming real-time data. A theoretical justification for the STA/LTA trigger based on the logarithm of the likelihood ratio can be found in Basseville and Nikiforov (1993).

Event detectors are configured so that the number of false detections is minimized. On the other hand the detector has to be sensitive enough in order to detect also smaller events. Therefore, any phase detector yields a considerable number of false detections and not all P phases are detected. Hence, the consistency of the detections at different stations has to be checked before the detection of an event is declared. For local seismic networks it is sufficient that within a short time interval of a few seconds P phases are detected at a certain number of stations. The time of the phase detection $\hat{T}_i$ at station i is interpreted as an estimation of the P- phase arrival time, which is, of course, afflicted with an error ε_i. $\hat{T}_i$ may be written as:

$$\hat{T}_i = T_0 + t_i + \varepsilon_i,$$

where T_0 is the source time and t_i is the travel time of a P wave to station i. The coincidence trigger detects an event, if for any combination of a minimum number of stations (typically three or four) the condition

$$|\hat{T}_i - \hat{T}_j| \leq \varepsilon$$

is met. ε is the maxmimum allowed difference between trigger times at neighboring stations. This coincidence trigger works satisfying for local networks, where the number of stations and the aperture of the network are not large. For regional and global networks this simple event detection algorithm has to be modified. Such a modified algorithm may be formulated as a grid search procedure. At every knot of a 3D grid a hypothetical hypocenter is assumed. The index k is introduced for a hypothetical hypocenter. T_{ki} denotes the expected P-phase arrival time at station i. The expected difference between arrival times at two stations for the assumed hypocenter k is

$$\Delta T_{kji} = T_{ki} - T_{kj} = t_{ki} - t_{kj},$$

where t_{ki} is the travel time from the hypocenter k to station i, that is in practise calculated using a reasonable background velocity model. The expected travel time difference ΔT_{kji} may serve as a condition that an event is detected at the hypothetical hypocenter k. If for a certain number of detections $\hat{T}_i$ occuring in the time interval $[t - \Delta t, t]$ the condition

$$|\hat{T}_i - \hat{T}_j - \Delta T_{kij}| \leq \varepsilon$$

is met, an event at the hypocenter k is declared. Only trigger times at predefined subsets of stations in the vicinity of the hypocenter k need to be checked in order to detect an event at hypocenter k. This algorithm is fast and yields robust prelimenary event locations even if the single-station phase detector produces a large number of false detections. This algorithm is implemented i.e. in the Earthworms phase associator “Binder” (Dietz, 2002).

A similar approach is proposed by Le Bras et al. (1994) in the widely used system Global Association (GA), where explicitly identified phases are assigned to synthetic earthquakes in overlapping circular grid cells with a complete global coverage. The performance of this algorithm relies on the correct phase identification, which is based on a combination of slowness and f-k analysis, polarization analysis, and frequency content.

Waveform correlation is used to identify seismic events. For finite-length time series from STA/LTA-triggered systems, Withers et al. (1998) propose the Local Waveform Correlation Event Detection System (LWCEDS). From observed waveforms envelopes are calculated using STA/LTA energy ratios and correlated with pre-calculated travel-time curves, which are transformed into processed time series by applying an envelope function to the arrival times for each distance bin. A single value for each station is summed, and the result is normalized by the number of stations, giving the final correlation value. After the summation over all given grid points and time intervals, respectively, the maximum sum is determined and an event is declared, if this maximum sum exceeds a certain threshold.

A grid search algorithm, which works without onset time detections, is proposed by Kao and Shan (2004). Within this Source-Scanning Algorithm (SSA) a brightness function is calculated by summing the absolute, normalized amplitudes observed at all stations at their predicted arrival times, i.e.

$$br(k,T) = \frac{1}{N}\sum_{i=1}^{N} \left| u_i(T + t_{ki}) \right|,$$

where u_i is the normalized seismogram at station i, t_{ki} is the predicted traveltime from point k the to station i of a particular phase with the largest observed amplitude (on regional scale S phase). The brightness is calculated of a point k at a specific time T and varies from 0 to 1. The brightness becomes 1 if all the largest amplitudes originate from a source at point k and time T. The spatial and temporal distribution of sources is identified by a systematic search througout the model space and time for the maximum brightness. For each source, this scanning algorithm results into a center of maximum brightness. Waveform based association algorithms may also be applied to the detection and location of tremors. The SSA algorithm was successfully applied to locate non-volcanic tremors in the northern Cascadia subduction zone (Kao and Shan, 2004).

In the case of earthquake data, the event detection is usually followed by a more precise automatic picking of P and optionally also S phases that allow to improve the event location.

16.3 Automated P-onset determination

After an event has been identified, an interval of the time series containing the seismic signal is usually cut out for detailed processing. For a precise event location, a picking algorithm is applied to the data to estimate P- and S-phase arrival times, respectively. In this section we review the most frequently applied and wide spread P-picking algorithms. We describe the algorithms and show applications to synthetic as well as to real examples in order to demonstrate properties and the performance of the picking algorithms. All pickers are applied to the same local, regional and teleseismic event example waveforms for reasons of comparison. Furthermore, the behaviour of the corresponding CFs are testet on synthetic data with instantaneous changes in amplitude, frequency, and phase, respectively, as the arrival of a body wave may be indicated by one or several of those changes. The synthetic examples are designed to investigate the properties of the CF rather than to simulate a P-wave arrival.

16.3.1 The Allen picker

Allen (1978, 1982) introduced the concept of *characteristic function* CF, where the "character" of the seismic trace is specified. The CF is obtained by one or several non-linear transformations of the seismogram and should increase abruptly at the arrival time of a seismic wave. In addition to the calculation of the CF the next steps of a picking algorithm are the estimation of the arrival time from the CF and the quality estimation.

Let x_i be the time series under investigation with first difference $\dot{x}_i$, Allen defined the following envelope function $E(t)$:

$$E_i = x_i^2 + C_i \cdot \dot{x}_i^2, \tag{16.1}$$

where C_i is a weighting constant with

$$C_i = \frac{\sum_{j=1}^{i} |x_j|}{\sum_{j=1}^{i} |x_j - x_{j-1}|} \tag{16.2}$$

to control the relative contributions of amplitude and derivative. For a harmonic x_i, equation (16.2) reduces approximately to

$$C_i = \frac{1}{f_i dt}, \tag{16.3}$$

where f is the frequency and dt the sampling frequency. If C_i in eq. (16.1) was squared, this envelope function would be an effective, recursive approximation of the squared envelope. That means the envelope function eq. (16.1) represents a fast but rough aaproximation of the waveform envelope.

In the context of this article, we refer to the definition of the CF by Baer and Kradolfer (1987), who defined the CF as the time series, to which the picker is applied. Note, that Allen (1978) uses the term CF slightly differently. According to his notation the envelope function *E(t)* represents the CF, though the picker is applied not to this function but to the STA/LTA ratio calculated using the envelope function. In order to illustrate properties of *E(t)* it is calculated for synthetic data with sudden changes in amplitude, frequency, and phase, respectively. From Fig. 16.1 it becomes obvious that only changes in amplitude are detected by Allen's CF.

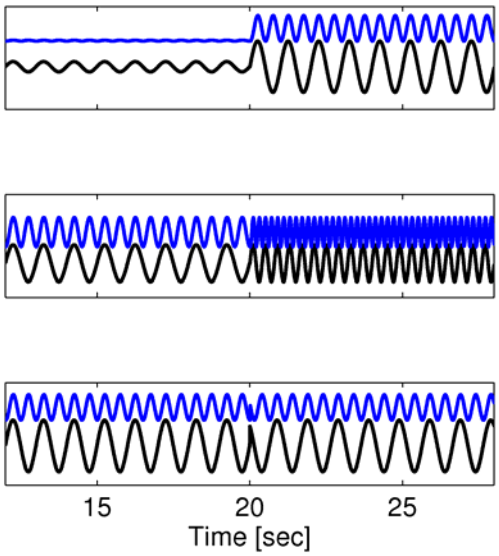

Fig. 16. 1 Allen's approximated squared envelope function (blue) for synthetic data (black) with a change in amplitude (top), change in frequency (middle) and change in phase (bottom). envelope function. That means $E(t)$ is sensitive to sudden changes in amplitude and frequency.

The following sophisticated algorithm is applied to $E(t)$ in order to obtain an arrival time estimate and to check the reliability of the pick. At first an STA/LTA criterion is used to detect possible arrival times. Then the duration of the signal is considered in order to distinguish between noise and P-wave arrivals and to reduce the number of false alarms. In the following description of the Allen picker we refer to the Fig. 16.2 and 16.3:

A short-term average (α) and a long-term average ($\beta \approx 100 \cdot \alpha[s]$) are calculated from the envelope function. If the STA/LTA ratio exceeds the reference level γ, the time is provisionally stored as a pick and the reference level γ is frozen (Fig. 16.2c). The picker now confirms or rejects the provisionally onset time by investigating the amplitudes of the raw seismogram. If low amplitudes (i.e. STA values exceed the continuation level δ) prevail, the picker assumes a short-term increase of noise and rejects the provisionally onset. If higher amplitudes prevail (i.e. STA values above the continuation level δ), the picker assumes a real seismic signal and estimates the length of this signal. To distinguish between short-term increases of noise and the seismic signal, the algorithm searches for the next zero crossing in the seismic trace. Reaching the next zero crossing, the picker starts counting the number *M* of observed peaks. *M* is incremented by 1 at each zero crossing. Using the number of observed peaks *M*, the continuation criterion δ is determined by $\delta = \beta(j) \cdot M$ and a "termination number" $L = 3 + 3/M$ (Fig. 16.2d,e) is calculated. δ and *L* are constantly increasing functions and serve as parameters to identify the length of the signal and hence to confirm the provisionally pick. In addition, also small amplitudes are counted: the short-term average α is compared with the continuation criterion δ. If α exceeds δ, a counter *s*, which Allen refers to as a "small count counter" and which counts the number of successive zero crossings occurring since α drops below δ, is reset. If α does not exceed δ, *s* is incremented by 1. If *s* becomes larger than the termination number *L*, the event is supposed to be over, otherwise the processing goes on until $s > L$. The length of the time interval for which $L > s$ serves as an estimate of the signal length (Fig. 16.2e). From Fig. 16.2d,e it is obvious, that the small count counter *s* increases significantly steeper than the termination number *L* as soon as the short-term average α remains below the continuation criterion δ. If the signal length exceeds a certain threshold t_{min}, the signal is supposed to be a seismic event, the pick is stored and optional post-processing starts. If the signal length is to short, the pick is removed, *s, L, M* and δ are reset and a new reference level γ is calculated.

In order to account for automatic quality and error assessment, Allen introduced a weighting scheme, based on the seismogram and the corresponding CF. The estimated weights of the determined P onsets may serve as input for the location routine HYPOINVERSE (2002, 2003), where weight-0 onsets denote excellent or impulsive (100 % weight), weight-1 very good (75 % weight), weight-2 good (50 % weight) and weight-3 intermediate onsets (25 % weight). Weight-4 picks are not used for location. The information needed are

- B, a measure of the noise level at the detection time;
- A_0, the trace amplitude at the detection time;
- D, the trace first difference at the detection time;
- A_1, A_2, A_3, the first three amplitude peaks.

For a weight-0 P onset ("excellent"), the detection has to meet the following criteria (after Allen, 1978):

1. $D > \sqrt{B}$,
2. $A_1 > 450$,
3. $A_1/\sqrt{B} > 4$,
4. $A_2 > 6\sqrt{B}$ or $A_3 > 6$.

These criteria are successively to be relaxed to obtain lower weights 1,2 and 3.

Tab. 16.1 Parameters to be adjusted for the Allen picker. The outer right colums represent the values of the parameters used for the example waveforms in Fig. 16.4.

Parameter	Remark	Values	Local	Regional	Tele
α	short-term-average of CF [s]	$0.01 < \alpha \leq 10$	0.1s	0.1s	10s
β	long-term-average of CF [s]	$2 < \beta \leq 50$	5s	5s	50s
C3	weighting of STA values	$0.2 < C3 \leq 0.8$	0.2	0.2	0.8
C4	weighting of LTA values	$0.005 < C4 \leq 0.05$	0.005	0.005	0.05
C5	LTA * C5 = δ	~ 5	2	2	3
tmin	minimum signal length required	1.5 [s]	3s	3s	40s

Fig. 16.4 shows applications of the Allen picker to waveforms of local, regional and teleseismic events. As shown by e.g. Küperkoch et al. (2010), this picking algorithm tends to pick somewhat early compared to an experienced analyst. Nevertheless, the Allen picker is a very robust and reliable algorithm. This sophisticated picking algorithm exploits informations provided by the CF as well as by the filtered seismogram. An advantage of the algorithm is that an automatic quality estimation of the P onset is implemented. The speed of the algorithm makes it also suitable for real-time picking of P phases.

When applying this algorithm, the parameters listed in Tab. 16.1 have to be tuned. These parameters are, of course, different for local, regional and teleseismic events and hence depend on the sampling frequency and the applied filter. The outer right columns in Tab. 16.1 show the values used for the presented example waveforms in Fig. 16.4, while the parameter ranges given in column “Values” are taken from Allen (1978).

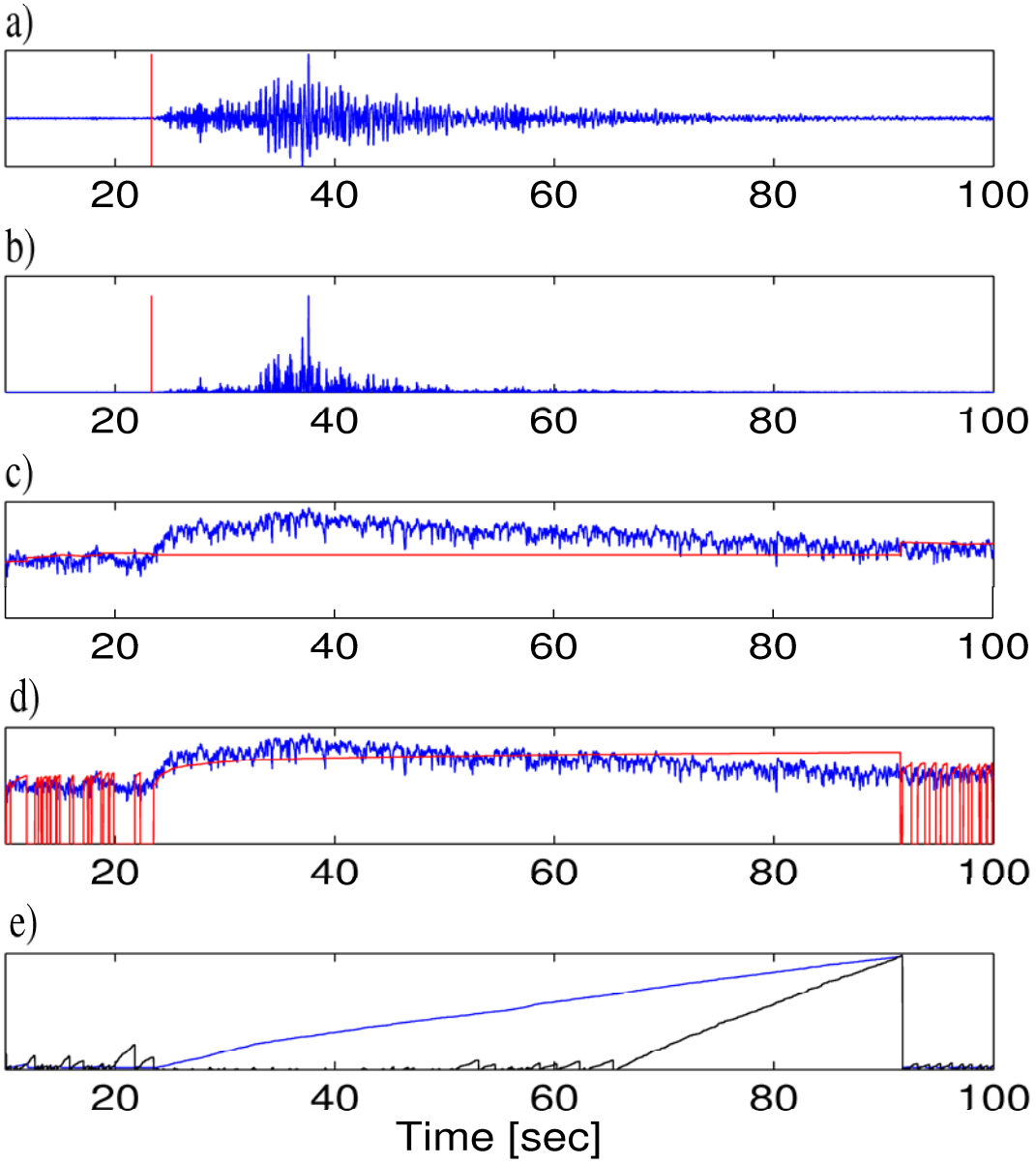

Fig. 16.2 Visualization of parameters and thresholds needed for the Allen picker. a) Bandpass filtered (Butterworth 3rd order, 2-10 Hz) vertical component seismogram (blue) with automatically estimated P onset (red). b) Corresponding approximated, squared envelope function (blue) with estimated P onset (red). c) STA values of Allen's envelope function (blue) and corresponding reference levels $\gamma = LTA \cdot C5$ (red). d) STA values of Allen's envelope function (blue) and corresponding continuation criterion δ (red). e) Termination number L (blue) and number of observed zero crossings with drops below the continuation criterion δ (black). When the termination number L and the number of observed zero crossings with STA < δ intersect, the signal is supposed to be over. For details, see text and flow chart (Fig. 16.3).

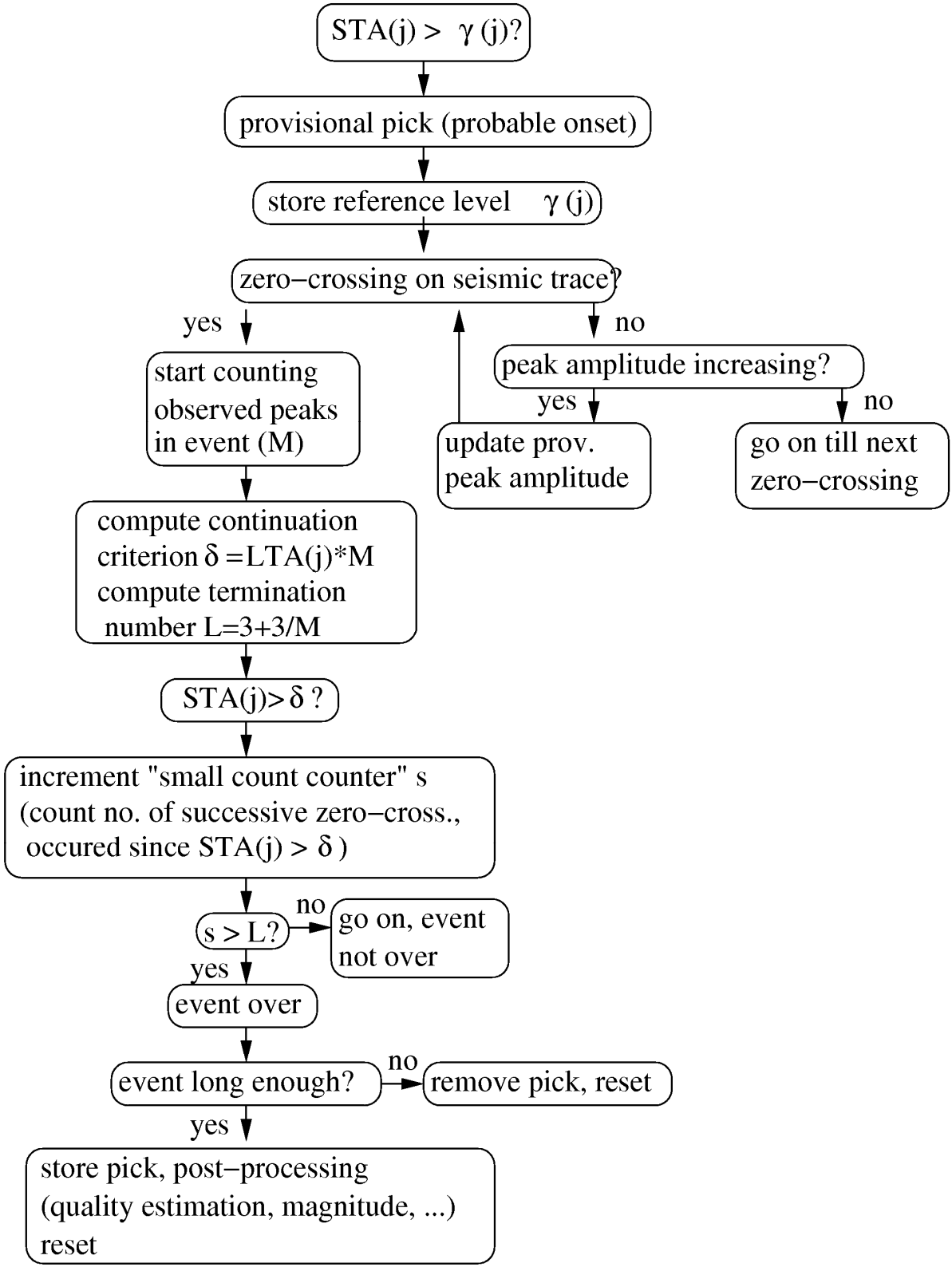

Fig. 16.3 Flow chart of Allen's picking algorithm. See text for details.

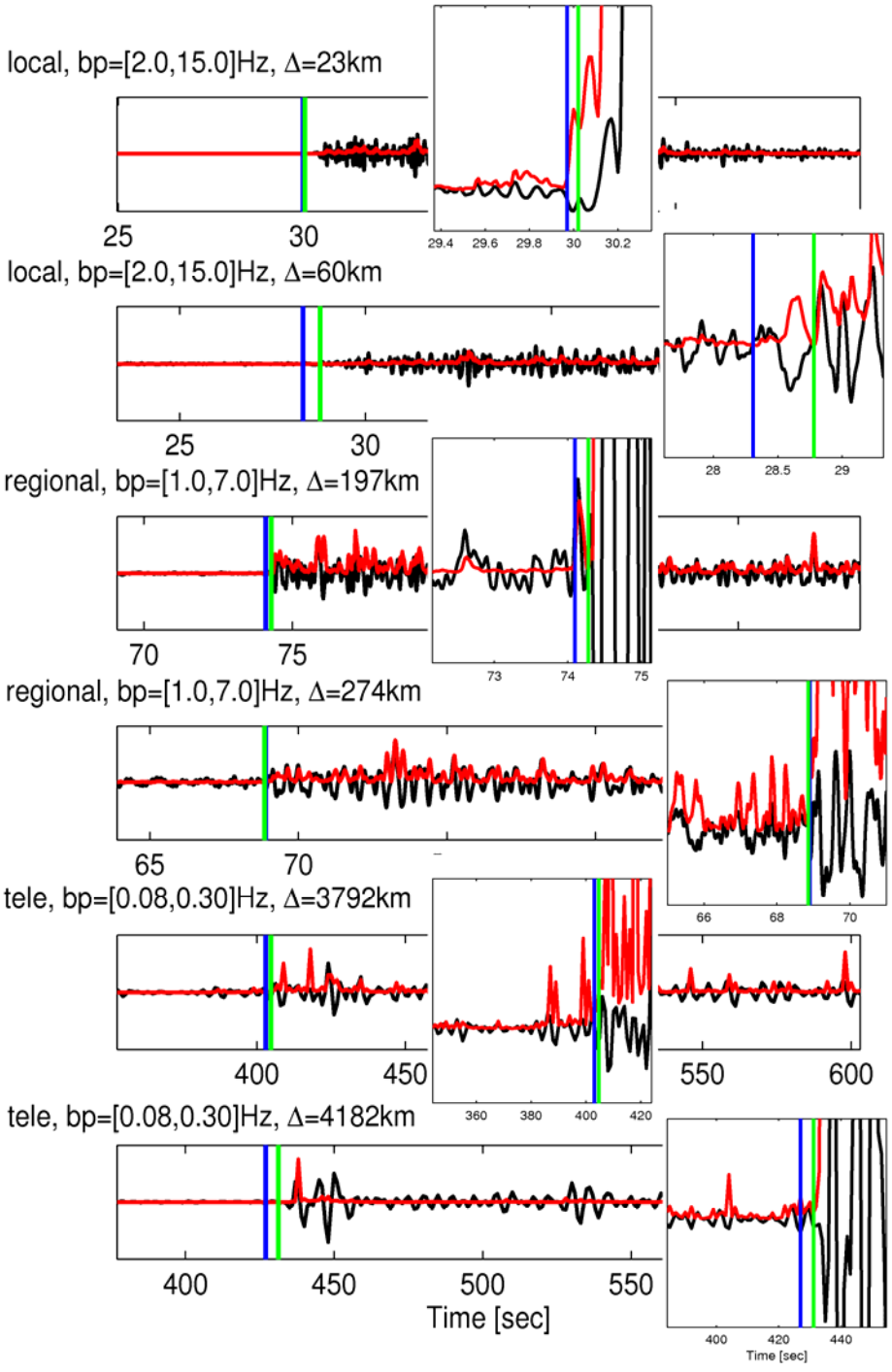

Fig. 16. 4 Automatically derived P onsets (blue vertical lines) using Allen's algorithm applied to waveforms of local, regional and teleseismic events (black). Applied filtering and epicentral distances are given at top of each panel. Allen's CF (STA values of squared envelope function) is plotted in red. To the right zoomed in portions of waveforms and CFs in the vicinity of the P onset. The green vertical lines indicate the corresponding manual picks. The differences between manual P readings and automatically estimated onset times are less than 0.5 seconds for these local and regional waveform examples. For the teleseismic event waveform examples the differences are 1.7 and 4.2 seconds, respectively.

16.3.2 The Baer and Kradolfer picker

Another widely used picking algorithm is the one proposed by Baer and Kradolfer (1987). This algorithm is frequently applied, e.g. by PITSA ("Programmable Interactive Toolbox for Seismological Analysis", Scherbaum and Johnson, 1992) and the picking system MannekenPix (Aldersons, 2004).

Baer and Kradolfer modified Allens' envelope function $E(t)$ to

$$E_i^2 = x_i^2 + \dot{x}_i^2 \frac{\sum_{j=1}^{i} x_j^2}{\sum_{j=1}^{i} \dot{x}_j^2}. \tag{16.4}$$

By squaring this envelope function and implementing the variance of $E(t)$, they obtain the following CF:

$$CF_i = \frac{E_i^4 - \overline{E_i^4}}{\sigma^2(E_i^4)} \tag{16.5}$$

where $\overline{E_i^4}$ is the mean of E_i^4 from j-th sample to i-th sample and $\sigma^2(E_i^4)$ is the variance of E_i^4 from sample j-th to sample i. As will be shown later, this CF is quite similar to the kurtosis, a parameter to quantify deviations from a Gaussian distribution. Tests on synthetic data using this CF are shown in Fig. 16.5. In contrast to Allen's squared envelope function this CF is sensitive to changes in amplitude, frequency as well as in phase.

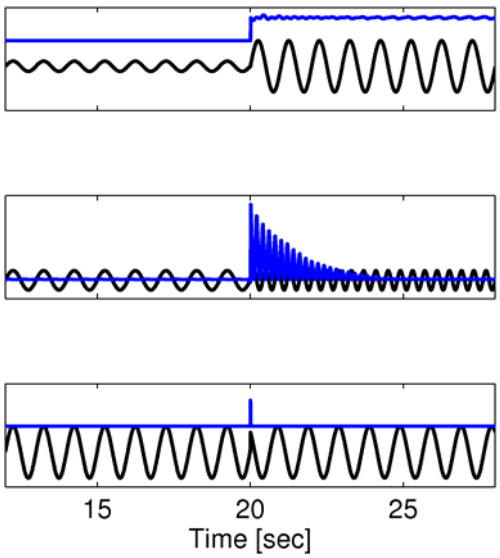

Fig. 16.5 The Baer and Kradolfer CF (blue) for synthetic data (black) with change in amplitude (top), change in frequency (middle) and change in phase (bottom). The CF proposed by Baer and Kradolfer is sensitve to the three types of changes

A pick flag is set if CF_i exceeds a threshold $\gamma \approx 10$. In order to avoid detecting short-term increases caused by noise, a signal is only accepted if the CF does not drop below the signal threshold for times larger than the dominating period. The variance $\sigma_i^2(E_i)$ is continuously updated, except when CF_i exceeds a second dynamic threshold $\delta \approx 2 \cdot \gamma$. If the CF decreases within a certain time "tup", the provisional pick is cleared. However, due to the complexity of seismic signals, drops of the CF below the threshold γ for "tdown" seconds are allowed.

Fig. 16.6 shows an example of the proposed CF, calculated for the recording of a local event. In this specific case the derived onset is somewhat late compared to the manual P reading.

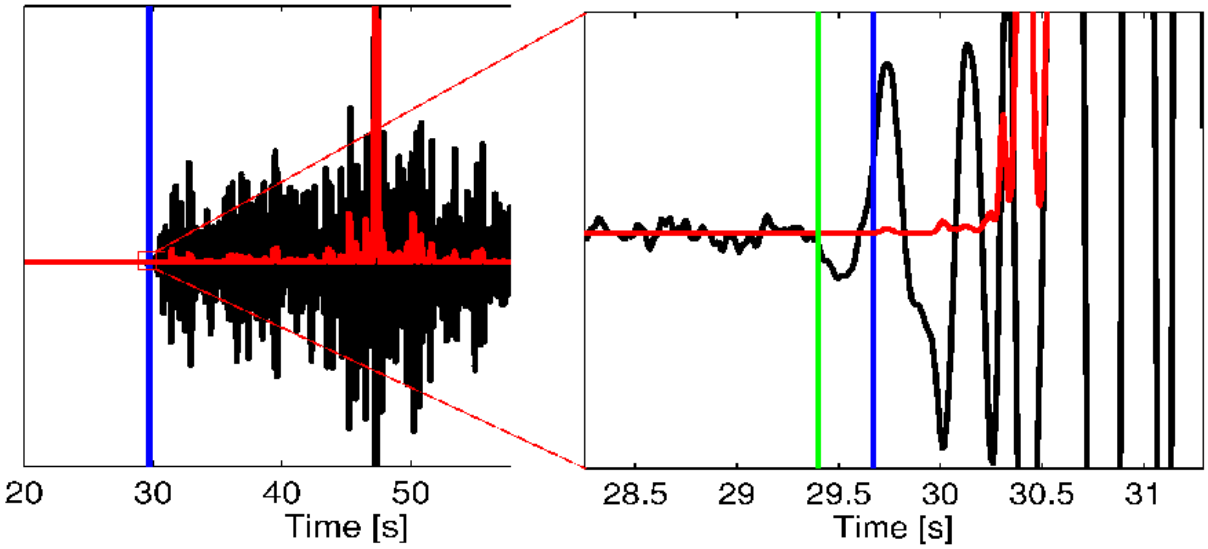

Fig. 16. 6 Example of the Baer and Kradolfer CF (red) calculated for a local event waveform (black). The blue vertical line indicates the automatically derived P onset, the green vertical line the manual P reading.

Tab. 16.2 shows the parameters to be adjusted when applying the Baer and Kradolfer picker, with the right-hand side columns giving the respective values used for the example waveforms of a local, regional and teleseismic event in Fig. 16. 7.

Tab. 16.2 Parameters to be adjusted when applying the Baer and Kradolfer picker with the respective case values of the parameters used for the example waveforms in Fig. 16.7.

Parameter	Remark	Values	Local	Regional	Tele
γ	threshold	10	10	5	2
δ	threshold for updating σ²	2*γ	20	10	10
tup	time [s] for CF to remain above threshold γ	>0.3	1.5	1.5	2
tdown	allowed time [s] for CF to drop below threshold γ without clearing pick flag	mean of corner frequencies	10	10	10

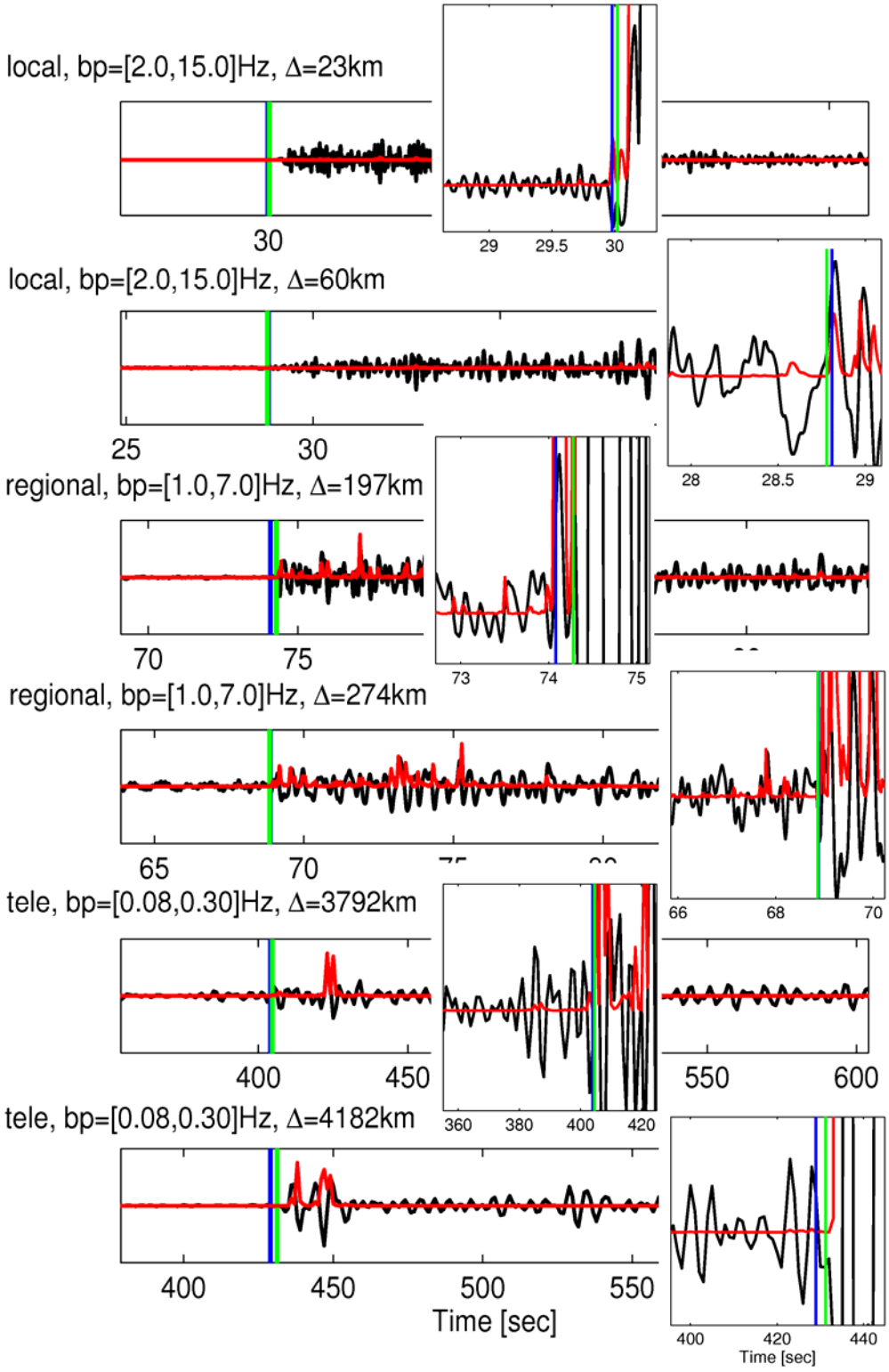

Fig. 16.7 Examples of waveforms of local, regional and teleseismic events and of the Baer and Kradolfer CF. Applied filtering and epicentral distances are given at the top of each panel. The green vertical lines indicate the manual P picks, while the blue vertical lines indicate the automatically estimated P-onset times. The differences between manual and automatick picks are less than 0.2 seconds for these local and regional waveform examples. For the two teleseismic event waveform examples the differences are 0.7 and 2.8 seconds, respectively.

All automatically derived P onsets are in good agreement to the corresponding manual ones. However, it has been shown that this algorithm tends to be somewhat late compared to manual P readings (e.g. Sleeman and van Eck 1999; Küperkoch et al. 2010). Aldersons (2004) integrated the Baer and Kradolfer picker in the picking system MannekenPix and introduces a delay correction. The idea for the correction is to shift the automatic onset back in time as long as the CF decreases significantly towards earlier samples. The delay correction stops when $CF_i - CF_{i-1}$ is smaller than 0.01, or when this condition cannot be met after moving back the onset by 3 samples. Aldersons states, that this simple correction usually provides "good to very acceptable results" for local earthquakes recorded by short-period instruments.

The Baer and Kradolfer picker is a fast and robust routine, which is also suitable for online detection. Baer and Kradolfer do not propose an automatic quality assessment. However, this algorithm yields high quality picks and was supplemented by the sophisticated quality assessment system MannekenPix (Aldersons, 2004; Di Stefano et al., 2006). Furthermore, the application of this algorithm is quite "user friendly" due to the low number of parameters to be set.

16.3.3 P-onset determination using Higher Order Statistics

When an earthquake signal arrives, the statistical properties of a seismogram change abruptly. Therefore, measurements of statistical properties in a moving window are suitable for the determination of a CF and subsequent estimation of arrival times. The statistical properties of the seismogram might be characterized by its distribution density function and by parameters like variance, skewness and kurtosis. The latter two are parameters of higher order statistics (HOS) and defined as follows (e.g. Hartung, 1991).

The expectation of a continuous distribution is given by

$$E[X] = \int_{-\infty}^{\infty} xp(x)dx \tag{16.6}$$

with the distribution function p(x) of the random variable X.

Using the expectation the statistic moment α of order k of the random variable X is defined as:

$$\alpha_k = E[X^k] = \int_{-\infty}^{\infty} x^k p(x)dx. \tag{16.7}$$

By analogy the central statistic moment m of order k is defined as:

$$m_k = E[(X - E[X])^k], k > 1. \tag{16.8}$$

The second central moment is the variance, the lowest moment yielding informations about the variability of a random variable:

$$Var[X] := E[(X - E[X])^2] = m_2. \tag{16.9}$$

The variance defines the mean power of the alternating part of an ergodian process.

Using the third central moment the skewness becomes:

$$S = \frac{E[(X - E[X]]^3}{E[X - E[X]]^{3/2}} = \frac{m_3}{m_2^{3/2}} \tag{16.10}$$

S becomes zero if the distribution is symmetrical. It becomes negative (positive) if the distribution shows outlayers to the left (right) of the expectation value. The skewness provides information about positive or negative deviations of the distribution density function from the expectation value.

The kurtosis is defined using the fourth central moment:

$$K = \frac{E[(X - E[X]]^4}{E[X - E[X]]^{4/2}} = \frac{m_4}{m_2^2}. \tag{16.11}$$

K is 3 for normally distributed random variables.

An estimation of a central moment from a random sample x_j, $j = 1,\mathsf{K}\ ,N$ is:

$$\hat{m}_k = \frac{1}{N}\sum_{j=1}^{N}(x_j - \bar{x})^k. \tag{16.12}$$

Estimations of the variance, skewness and kurtosis are hence given by:

$$\hat{\sigma}^2 = \hat{m}_2 = \frac{1}{N}\sum_{j=1}^{N}(x_j - \bar{x})^2 \tag{16.13}$$

$$\hat{S} = \frac{\hat{m}_3}{\hat{m}_2^{3/2}} \tag{16.14}$$

$$\hat{K} = \frac{\hat{m}_4}{\hat{m}_2^2} \tag{16.15}$$

Tab. 16.3 shows some example spot checks and their corresponding estimates of variance, skewness and kurtosis. Especially skewness and kurtosis show the potential to detect even small outliers. The first two examples show symmetrically distributed spot checks. The estimated skewness is zero. In the second example the variance increases, though no outlier distorts the distribution. The skewness remains zero and kurtosis increases only slightly. In the third example the outlier is clearly indicated by skewness and kurtosis, while the estimate of the variance remains the same as for the second example.

Tab. 16.3 Examples of spot checks and corresponding values for variance, skewness and kurtosis.

Spot Check	$\hat{\sigma}^2$	$\hat{S}$	$\hat{K}$
[1,–1,1,–1]	1	0	1
[1,–1,2,–2]	2.5	0	1.36
$[1,-1,1,-\sqrt{7}]$	2.5	-1.11	2.08

Fig. 16.8a shows the distribution density function of real background noise. Variance, skewness and kurtosis are calculated in a moving window with a length of 20 seconds. Skewness and kurtosis indicate an almost Gaussian distribution. As soon as the moving window reaches a signal onset (Fig. 16.8b), the shape of the distribution density function changes abruptly and deviates from a Gaussian distribution. Kurtosis and skewness increase strongly.

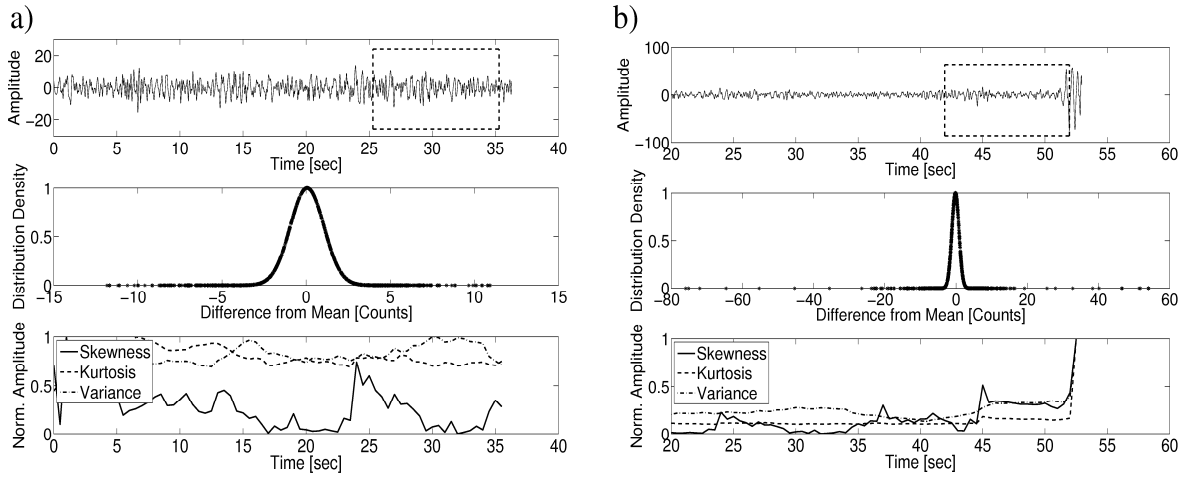

Fig. 16.8 a) Background noise (top) and corresponding distribution density function (middle), calculated in a moving window of 20 seconds length (dashed box). Bottom: estimated variance, skewness and kurtosis (normalized).
b) The moving window reaches a signal onset. The distribution density function is no longer Gaussian shaped, variance, skewness and kurtosis increase strongly.

Longbottom et al. (1988) used higher order statistics (HOS) for the deconvolution of seismic data and called their algorithm a simplified minimum entropy deconvolution method. Saragiotis et al. (2002) suggest to estimate skewness and kurtosis in a moving window to pick P-wave arrival times. Gentili and Bragato (2006) and Gentili and Michelini (2006) used skewness, kurtosis and a combination of skewness and kurtosis and their time derivatives as input for a neural network trained to estimate P-arrival times. Groos and Ritter (2009) used higher order statistics to classify broadband urban noise (USN).

Using eqs. (16.14) and (16.15), skewness and kurtosis are estimated in a moving window. This yields the CF from which the arrival times of the P wave is determined. In order to make the calculation fast, a recursive procedure is suggested:

Let $\{x(j)\}$ be a zero-mean, stationary process, T the length of the moving window and

$$N = T/dt + 1, \tag{16.16}$$

the number of samples of the moving window, with dt being the sampling interval. The actual value for the central moment of order k of the moving window is:

$$\hat{m}_k(j) = \frac{1}{N}\sum_{l=0}^{N-1} x_{j-l}^k. \tag{16.17}$$

Its estimate at sample j may be calculated from the previous estimate at sample $j-1$:

$$\hat{m}_k(j) = \hat{m}_k(j-1) - (x^k(j-N) + x^k(j))/N. \tag{16.18}$$

Using eqs. (16.14) and (16.15) skewness and kurtosis are calculated from recursively estimated central moments. Computation times may be decreased by a factor of about 10.

In Fig. 16.9 CFs calculated using skewness and kurtosis are compared to the CF of an STA/LTA for synthetic data with a change in amplitude, frequency and phase, respectively. The test indicates the strong sensitivity of skewness and kurtosis for changes in amplitude. While changes in frequency are detected by skewness and kurtosis, there is only a marginal detectability of changes in phase.

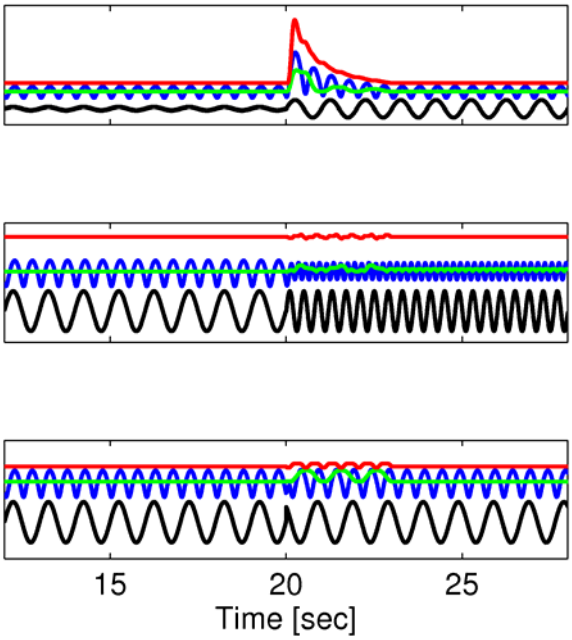

Fig. 16.9 Tests on synthetic data (black) with changes in amplitude (top), frequency (middle) and phase (bottom). Green: skewness, red: kurtosis, blue: STA/LTA.

From the CF arrival times are determined. Küperkoch et al. (2010) propose a sophisticated, iterative algorithm, which is organized into four stages. A detailed description of the algorithm and the parameter settings is given in their paper. The algorithm might briefly be described as follows:

(1) A CF using skewness or kurtosis is calculated from a bandpass filtered waveform (2-10 Hz for local to regional events). In analogy to Maeda (1985) the Akaike Information Criterion (AIC, Akaike, 1971) is calculated, yielding a first approximate P onset, which is the minimum of the AIC function (Fig. 16.10b).

(2) Using this preliminary P onset, the CF is recalculated around the initial onset in a smaller window, considering a higher frequency content (e.g. 2-15 Hz). The picker searches then for a common local minimum of a smoothed and the unsmoothed CF as this indicates a P-wave onset. The search is carried out to the right and to the left of the intial P onset within a certain pick window. If local minima are found on both sides of the initial P onset, the lower common minimum with lower amplitude of the CF is assumed to coincide with the true P-arrival time (Fig. 16.10c).

(3) For automatic quality assessment the slope of the CF right after the determined phase onset and the signal-to-noise ratio (SNR) serve as two quality criteria (Fig. 16.10c).

(4) Errorneous P onsets are found by checking the signal length and comparing the energy of the vertical component with the energy of the horizontal components to get rid of S picks, spuriously picked as P onsets. Furthermore, the consistency of automatically picked P onsets is checked. The difference between the picks should be lower than a certain threshold and the individual P picks should not have a strong influence on the estimate of the variance of the P picks. This is tested by a Jackknife procedure.

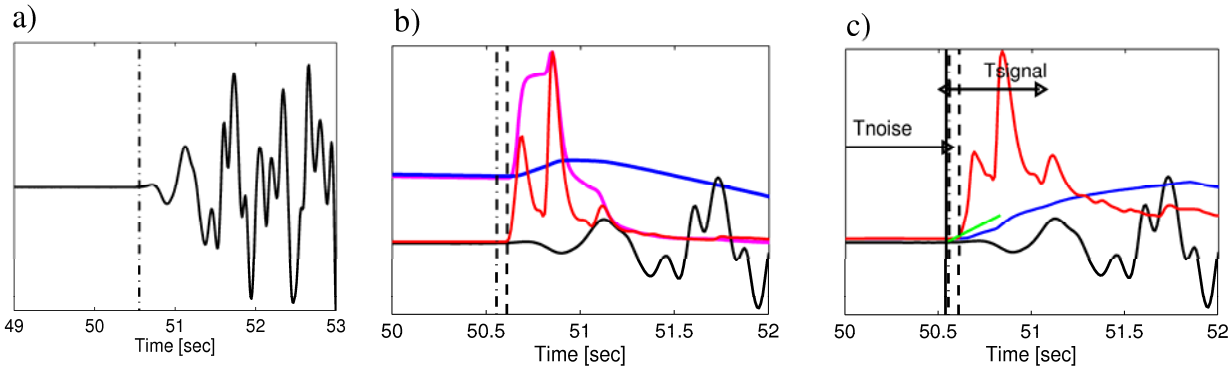

Fig. 16.10 Automatic determination of a P onset in a 2-10 Hz bandpass filtered, local event waveform (a, black) using the iterative picking algorithm proposed by Küperkoch et al. (2010). The manual P reading is indicated by the dashdotted vertical line. (b) Zoomed in portion of the waveform (black), also showing the CF calculated using kurtosis (red), the unsmoothed AIC function (cyan) and the smoothed AIC function (blue). The initial P onset (dashed vertical line) is determined from the two AIC functions. (c) Zoomed in waveform (black), recalculated, unsmoothed CF (red) using kurtosis, calculated from 2-15 Hz bandpass filtered data, and recalculated, smoothed CF (blue). The green line indicates the slope fitted to the unsmoothed CF. The noise window *Tnoise*and the signal window *Tsignal* are used for SNR estimation. *Tnoise* is 2 seconds.

Fig. 16.11 shows applications of the picking algorithm using kurtosis to local, regional and teleseismic events. For local and regional waveform examples the automatically derived P onsets show less than 0.2 seconds deviation from the manual picks. For the teleseismic waveform examples the differences are 0.7 and 3.2 seconds, respectively.

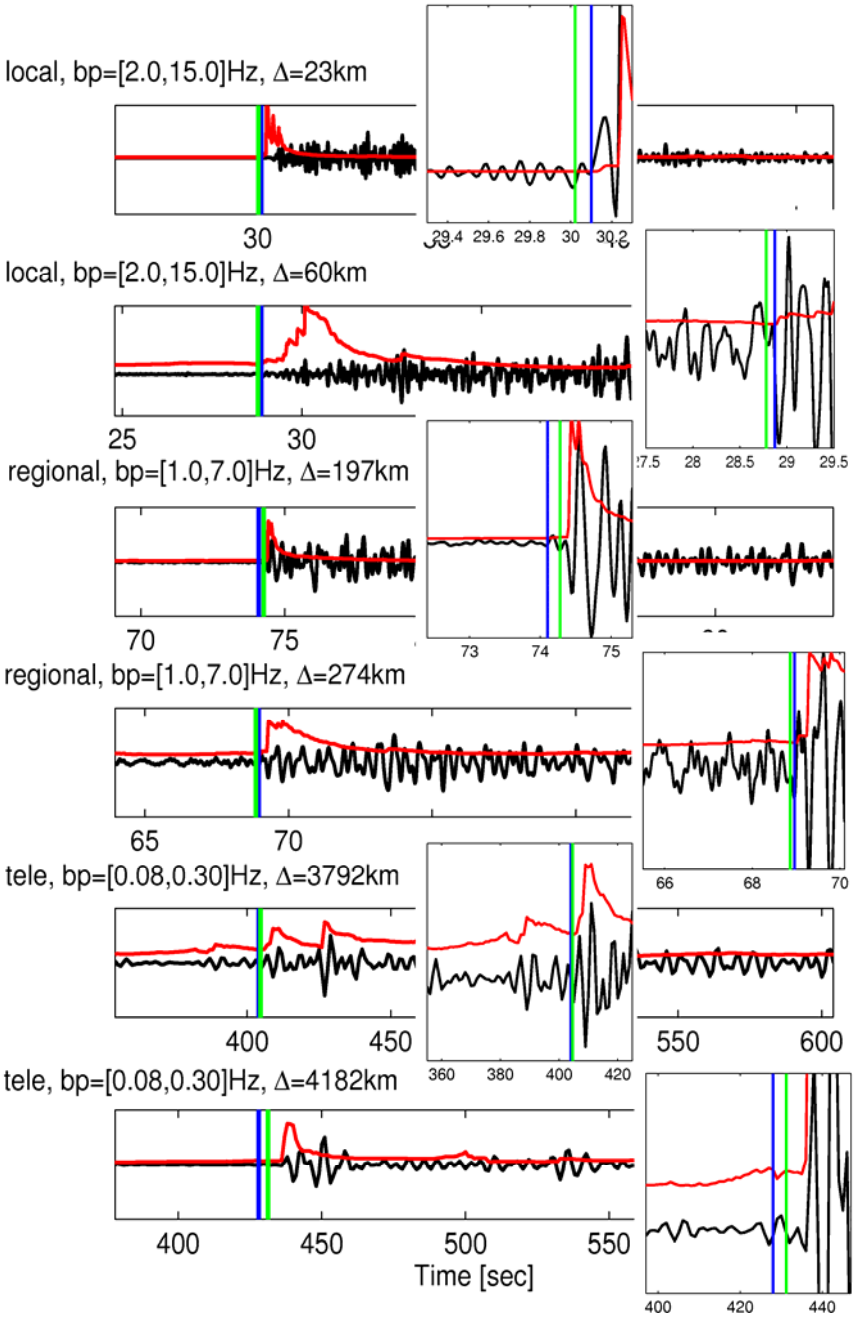

Fig. 16.11 Examples for waveforms of local, regional and teleseismic events and the corresponding characteristic functions determined using kurtosis. Applied filtering and epicentral distances are given at the top of each panel. The green vertical lines indicate the manual P picks, the blue vertical lines the automatically derived P-onset times. While the differences between manual picks and automatically P-arrival time estimates are less than 0.2 seconds for the local and regional waveform examples, the differences for the teleseismic waveform examples are 0.7 and 3.2 seconds, respectively.

Skewness and kurtosis are very sensitive to changes in amplitude, while changes in frequency or phase are hardly detectable. The proposed picking algorithm yields very accurate P readings in combination with a reliable quality assessment. Due to the recursive calculation of higher order central moments, this approach is also suitable for onset detection. The length of the moving window for kurtosis and skewness calculation typically range between 2 and 20 seconds, depending on the dominating frequency from which the window should include not less than about approx. 1.5 oscillations.

Skewness and kurtosis are successfully applied by Saragiotis et al. (2002) to 44 seismic events. The corresponding P onsets are compared to manual derived P onsets as well to automatically derived P onsets using Allen's algorithm (see sub-section 16.3.1). The comparison yields better results for the HOS approach. Furthermore, a large scale comparison was performed by Küperkoch et al. (2010) using more than 3000 manually derived P onsets of local to regional events. They found for their data set excellent results when using kurtosis and outperformed the additionally applied picking algorithms proposed by Allen and Baer and Kradolfer (see sub-section 16.3.2).

16.3.4 The AR-AIC picker

A stochastic time series, in which the *i*-th sample is described as a linear combination of the *p* predecessors, is called an autoregressive process of order *p*, which can be abbriviated as AR(*p*). The mathematical representation is

$$x_m = \sum_{m=1}^{p} a_m x_{m-j} + \varepsilon_m \,, \tag{16.19}$$

with *E[x]=0,* where a_m are the coefficients or parameters of the AR process and ε_m white noise. Eq. (16.19) can be rewritten as

$$x_m = a_1 x_{m-1} + \mathsf{L} \; + a_p x_{m-p} + \varepsilon_m . \tag{16.20}$$

When an earthquake signal arrives, the characteristics of a seismogram, such as variance and the spectrum, change abruptly. For the estimation of a phase arrival, it is assumed that each of the segments before and after the arrival of the seismic wave is stationary and might be expressed by an autoregressive model as follows (e.g. Kitagawa et al., 2001):

noise model (1st, pre-onset segment, for *n=1,...,k):*

$$x_n^1 = \sum_{m=1}^{M} a_m^1 x_{n-m} + \varepsilon_n^1 \tag{16.21}$$

signal model (2nd, post-onset segment, for *n=k+1,...,N*);

$$x_n^2 = \sum_{m=1}^{L} a_m^2 x_{n-m} + \varepsilon_n^2 \tag{16.22}$$

where $k+1$ is the change point between the two segments (i.e. the phase arrival), a_m^1 and a_m^2 are the AR coefficients, ε_n^1 and ε_n^2 represent gaussian distributed noise in the two segments, and M and L are the orders of the AR processses of the noise and the signal model, respectively, which are all unknown parameters. In the following we briefly outline the estimation of these parameters and show an application of locally, stationary segments and its description with autoregressive processes.

Waveforms of seismic phases show usually a higher complexity than that of the preceding noise and should therefore be described by a larger number of AR parameters, i.e., by an AR model of higher order p (e.g. Leonard and Kennett, 1999). Leonard and Kennett (1999) obtain the order of the AR process by fitting AR power spectra to noise and signal power spectra. Another approach of estimationg the order of an AR process (called model identification) is the use of the (empirical) partial autocorrelation function (PACF, e.g. Box et al., 1994). While the (empirical) autocorrelation function (ACF) gives the relation between the actual value of a time series and a later (earlier) value (delayed with time lag τ), not taking into account the influence of interjacent values, the PACF gives the direct correlation between lag-k distant values by removing the influence of interjacent values. For an AR process of order p the PACF will be nonzero for time lags l less than or equal p and zero for time lags $l>p$ and hence gives informations about the order of an AR process. Akaike (1970) proposed the final prediction error (FPE) to estimate the model order.

Fig. 16.12a) and 16.12b) show the pre-event noise window, the signal onset and the corresponding empirical ACF as well as the empirical PACF, from which the order of the process is estimated. The order of the time series incorporating the signal onset is much higher than that for the noise window. The PACF is assumed to be zero if the PACF is smaller than the standard S.E., which is $S.E. = 1/\sqrt{N}$ (e.g. Box et al., 1994), where N is the number of observations. PACF and FPE yield the same model orders.

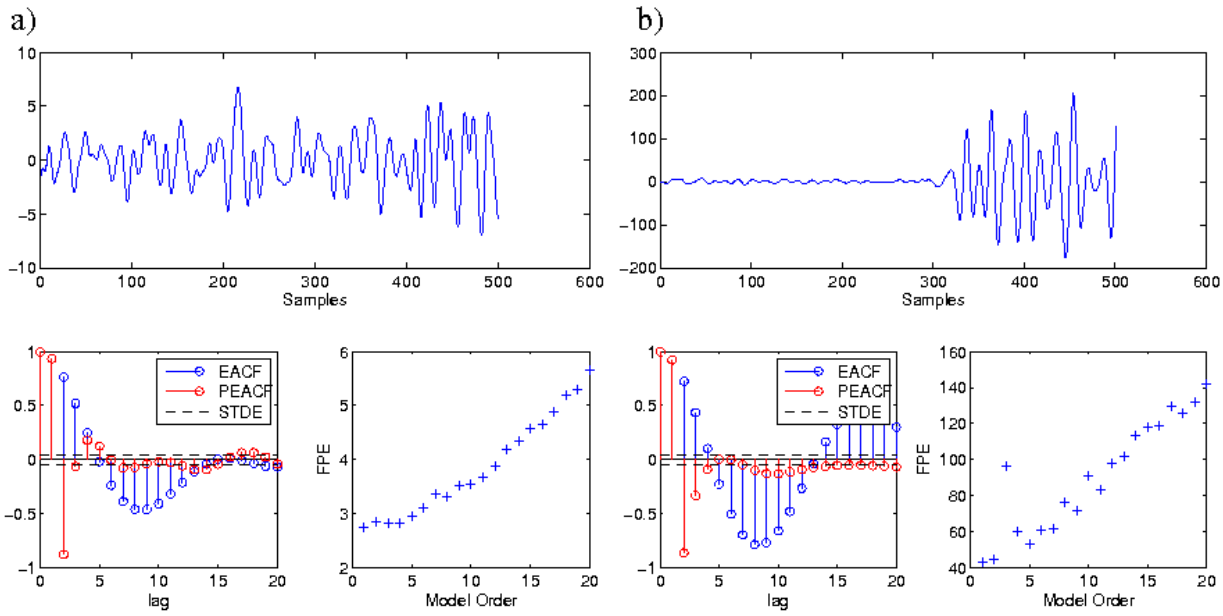

Fig. 16.12 a) Pre-event portion of a seismogram, corresponding ACF and PACF for sample lags 0 to 20, and FPE as a function of model order. The order of the AR process can be obtained from the PACF. The last value of the PACF which is larger than the standard error (dashed line) occurs at sample lag 3. The order of the AR process is therefore 3. The FPE

function also gives a local minimum at model order 3. **b)** Pre-event portion, seismic phase onset, corresponding ACF and PACF for sample lags 0 to 20, and FPE as a function of the model order. The order of the AR process is estimated to be 5, as the last value of the PACF, which is larger than the standard error, is at sample lag 5, indicating a higher complexity of the seismic signal compared to the preceeding noise. Also the FPE gives a local minimum at model order 5.

However, the estimation of the order of an AR process is very uncertain, and hence in most AR applications a fixed AR order is used, estimated with the introduced procedure or by trial and error (e.g. Leonard and Kennett, 1999).

The so called autoregressive-Akaike-Information-Criterion-picker (AR-AIC) proposed by Sleeman and van Eck (1999) is based on the work by Akaike (1971, 1974), Morita and Hamaguchi (1984) and Takanami and Kitagawa (1988). A longer time series is divided into two locally stationary segments each modeled by an AR process. The first segment represents noise, the second segment contains the signal. The picking algorithm can be described by five steps: (1) Bandpass filtering of the seismogram, (2) detection of a seismic phase using an STA/LTA detector, (3) estimation of two sets of AR parameters, namely for noise and signal, respectively, (4) calculation of two prediction errors using the AR parameters for noise and signal, respectively, (5) the minimum of the two-model AIC indicates the arrival time. For the following detailed description of the picker algorithm we assume that due to a first rough estimation of the P-wave arrival time the time series $x_n = x_1, \mathsf{L}\ , x_N$ can be divided into two subseries: the first represents noise, the second the seismic phase (signal). Thus, starting point for the following derivation are eqs. (16.21) and (16.22). Furthermore, we assume a fixed order *M* for both models, estimated by trial and error or the use of the PACF.

As we assume Gaussian distributions of ε_n^1 and ε_n^2, we can write for the two corresponding likelihood functions:

$$l(\varepsilon_n^1) = \frac{1}{\sigma_1\sqrt{2\pi}} e^{-\frac{(\varepsilon_n^1)^2}{2\sigma_1^2}} \tag{16.23}$$

$$l(\varepsilon_n^2) = \frac{1}{\sigma_2\sqrt{2\pi}} e^{-\frac{(\varepsilon_n^2)^2}{2\sigma_2^2}} \tag{16.24}$$

The approximate likelihood of the locally stationary AR model in the intervals $[M+1, k]$ and $[k+1, N-M]$ is hence given by

$$L(x, M, a_m^i, \sigma_i^2 (i=1,2)) = \prod_{i=1}^{2} \left(\frac{1}{\sigma_i^2 2\pi} \right)^{\frac{N_i}{2}} exp\left(-\frac{1}{2\sigma_i^2} \sum_{n=p_i}^{q_i} \left(x_n - \sum_{m=1}^{M} a_m^i x_{n-m} \right)^2 \right) \tag{16.25}$$

with $p_1 = M+1,\ p_2 = k+1,\ q_1 = k,\ q_2 = N-M,\ n_1 = k-m$ and $n_2 = N-M-k$.
The condition for maximum likelihood estimates of the model parameters is

$$\frac{\partial log(L(x,M,a_m^i,\sigma_i^2)}{\partial(a_m^i,\sigma_i^2)}=0, \tag{16.26}$$

which yields

$$\sigma_{i,max}^2=\frac{1}{n_i}\sum_{j=p_i}^{q_i}\left(x_j-\sum_{m=1}^{M}a_m^i x_{j-m}\right)^2. \tag{16.27}$$

Note, that the second sum is equivalent to the prediction error.

By substituting eq. (16.27) into eq. (16.25), the maximum of the logarithmic likelihood function $log(L(k,x,M,a_m^i,\sigma_i^2))$ for the two models as function of division point k becomes:

$$log(L(k,x,M,a_m^i,\sigma_i^2))=-\frac{1}{2}(k-M)log(\sigma_{1,max}^2)-\frac{1}{2}(N-M-k)log(\sigma_{2,max}^2)+C \tag{16.28}$$

where C is a constant. In the case of the locally stationary AR model, the AIC, which is a criterion for the selection of the best statistical model, is given by (Akaike, 1971):

AIC = -2(maximum log likelihood) + 2(number of parameters),

where the number of parameters is given by the model order. For the merging point *k,* which separates the two models, the AIC becomes:

$$AIC(k)=AIC^1+AIC^2 \tag{16.29}$$

and thus:

$$AIC(k)=(k-M)log(\sigma_{1,max}^2)+(N-M-k)log(\sigma_{2,max}^2)+C_1 \tag{16.30}$$

where C_1 is a constant. The minimum of the AIC points then to the optimal seperation time of the two stationary time series and indicates the arrival time of the phase. The AR coefficients a_m^i in eq. (16.27) are estimated in advance seperately for the noise and the signal model, repsectively. This is usually accomplished by either the Yule-Walker approach (e.g. Box, 1994), Burgs algorithm (Burg, 1975), or the least-squares approach.

In the following the AR-AIC picker is applied to synthetic and real test waveforms. The AR coefficients of the noise and the signal models are estimated in windows of 4 seconds length. The window of the noise model starts 4 seconds before the initial estimate of the arrival time. The window for the estimation of the AR parameters of the signal starts at the initial estimate of the arrival time (Fig. 16.13, top). The picker searches for the minimum in eq. (16.30) in a time window of 12 seconds length starting 8 seconds before the initial STA/LTA detection (Fig. 16.13, bottom). Sleeman and van Eck (1999) fixed the order of the two AR models to 8. Leonard (2000) used an order 4 AR model for both signal and noise.

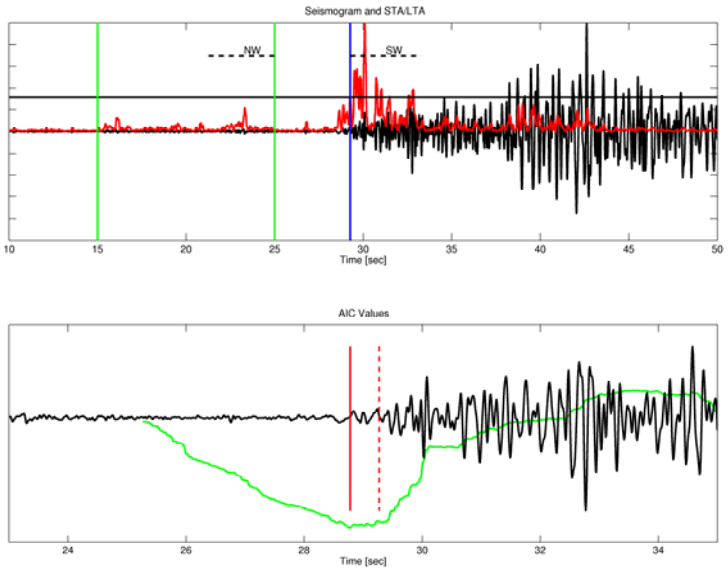

Fig. 16.13 Top: Waveform of a local event (black) and an initial P-onset detection (blue) derived from STA/LTA ratios (red). The green vertical lines indicate the time interval for noise level estimation. The dashed lines denote the time windows for determination of AR coefficients for the noise and the signal model, respectively (NW and SW).
Bottom: Waveform (black) around the initial STA/LTA pick (red,dashed line) and the automatically determined P onset (red line). Green: The AIC as a function of the merging point k, determined using eq. (16.30).

Fig. 16.14 shows the results for the synthetic data. For this test, we reduced the assumed order of the AR process to 2. The test shows clearly the potential of AR algorithms to detect changes in amplitude, frequency as well as in the phase.

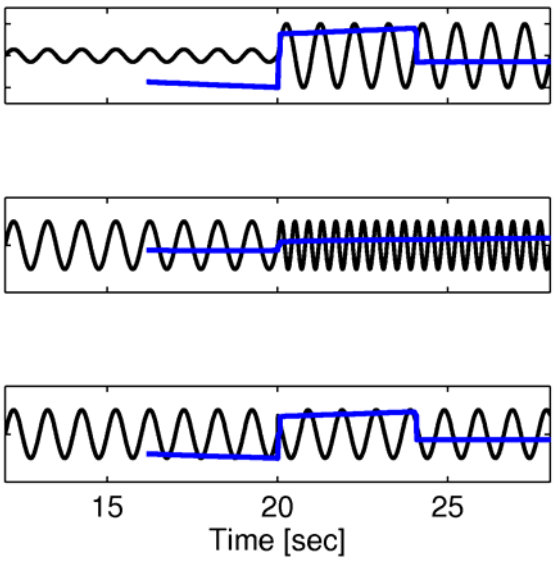

Fig. 16.14 AR-AIC (red) as function of the merging point k for synthetic data (black) with changes in amplitude (top), changes in frequency (middle), and changes in phase (bottom). The assumed order of the AR process is reduced to 2. Changes in the time series are recognized in all three cases.

Tab. 16.4 Parameters to be adjusted for the AR-AIC picker. Parameter settings applied for STA/LTA trigger used to get initial the P onset are not shown. The outer right columns represent the values used for the example waveforms in Fig. 16.15.

Parameter	Remark	Values	Local	Regional	Tele
tseg1	length of 1st segment for calculating AIC(k) [s]	4	8	8	50
tseg2	length of 2nd segment for calculating AIC(k) [s]	4	4	4	40
tnoise	length of noise window for AR-coefficient determination [s]	4	4	4	50
tsignal	length of signal window for AR-coefficient determination [s]	4	4	4	50
offset1	offset between initial pick and *tnoise* [s]	4	4	4	50
offset2	offset between initial pick and *tsignal* [s]	0	0	0	0

Fig. 16.15 shows applications of the AR-AIC picker to real local, regional, and teleseismic waveform data. Tab. 16.4 summarizes the parameters used for the example waveforms in Fig. 16.15 and the parameters proposed by Sleeman and van Eck (1999).

One shortcoming of this picker is the dependency on the STA/LTA trigger, which may be exchanged by a more robust procedure. The weighting scheme based on signal-to-noise ratios is useful for detecting false picks, but does not yield reliable quality estimates of the onset. However, the shape of the AIC function depends on the "sharpness" of the onset and could thus serve as a quality criterion (Diehl et al., 2009b, electronic supplement). The AR-AIC picker is more expensive but also more powerful than the Allen picker and the Baer and Kradolfer picker due to its strong sensitivity to changes in the waveform. Furthermore, this picking algorithm represents a robust tool for the identification of a first arrival.

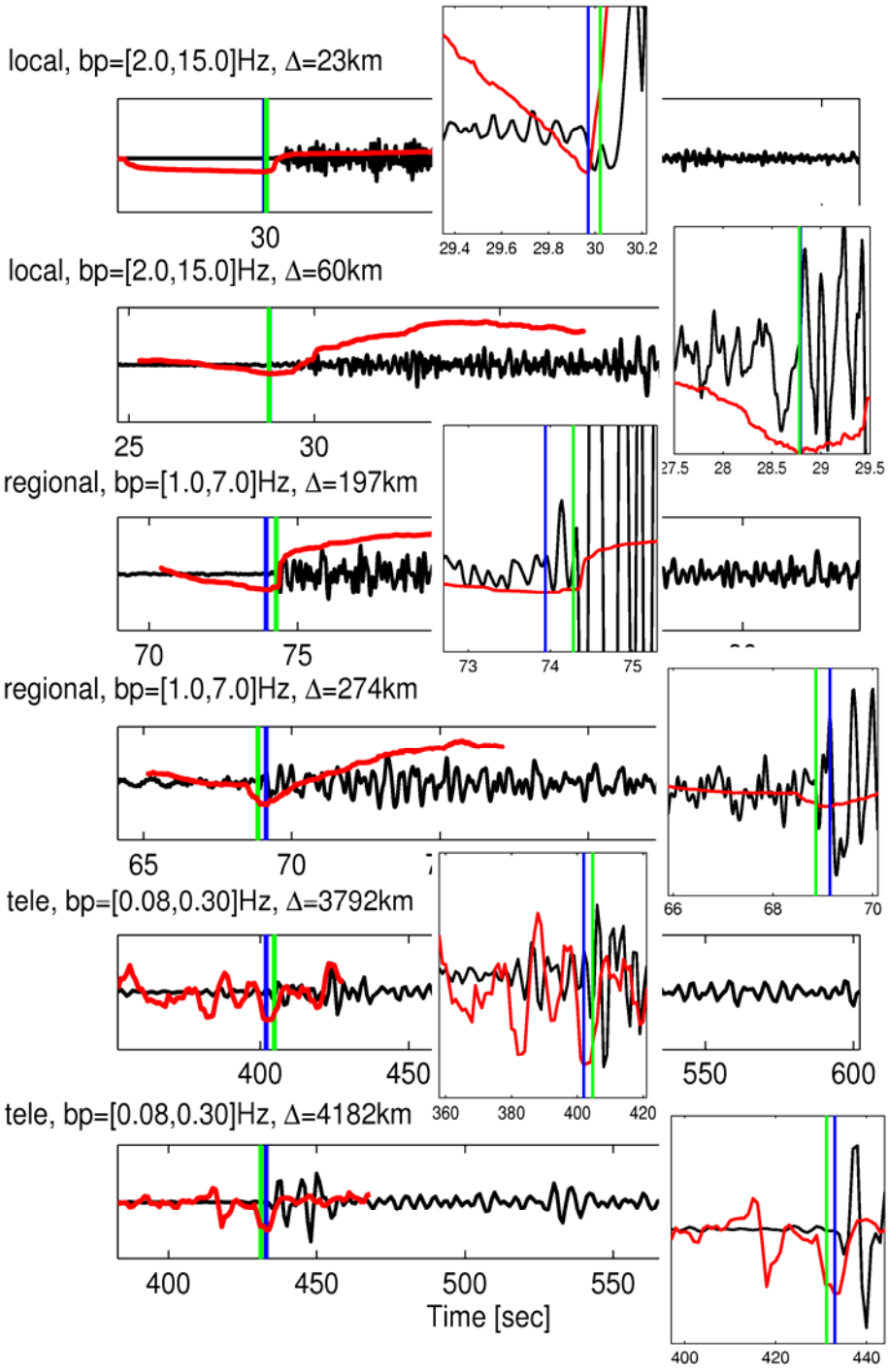

Fig. 16.15 Waveform examples of local, regional and teleseismic events and the corresponding characteristic functions for the AR-AIC picker proposed by Sleeman and van Eck (1999). Applied filtering and epicentral distances are given at top of each panel. The inital pick is determined by a STA/LTA detector. AIC as a function of the merging point is shown in red. The blue vertical lines denote the automatically determined P-phase arrival times, the green vertical lines the manual P picks. For local event waveform examples, the differences between manual picks and automatically estimated P-arrival times are 0.05 and 0.01 seconds, for regional waveform examples 0.34 and 0.28 seconds, and for teleseismic waveform examples 2.7 and 1.8 seconds, respectively.

16.3.5 Discussion of presented P-picking algorithms

The previous section presented four widely used P-picking algorithms in great detail. However, for potential users it might be difficult to decide which algorithm to choose for his certain data set. Therefore, we try to summarize the pros and cons of the four presented algorithms.

The Allen picker is a fast and robust algorithm, which also accounts for automatic quality assessment. However, as this algorithm is amplitude based only, it might miss emergent P onsets. A comparative study by Küperkoch et al. (2010) showed that this algorithm tends to pick somewhat early compared to what an analyst would pick.

The Baer and Kradolfer picker is also very fast and robust and quite user-friendly, as this algorithm only needs 4 input parameters. A shortcoming of this algorithm is the missing automated quality assessment. Several comparative studies (Sleeman and van Eck 1999, Aldersons 2004, Küperkoch et al. 2010) showed that this picking algorithm tends to be somewhat late compared to manual P picks.

Though only amplitude based too, higher order statistics are quite sensitive even to emergent P onsets. In combination with a sophisticated picking algorithm (e.g. Küperkoch et al. 2010), which exploits the entire information provided by the determined CF, yields excellent results. If precisely tuned, the automated quality assessment proposed by Küperkoch et al. (2010) gives similar weights as the analysts. However, the choice of the various parameters needed for this sophisticated algorithm is quite difficult and needs some experience.

The AR-AIC picker is a highly sophisticated picking algorithm based on information theory. The algorithm is computationally quite expensive and hence much slower than the other presented picker. In the discussed version by Sleeman and van Eck (1999) the initial P onset is derived from an STA/LTA detector, which might miss emergent P arrivals or P-phase arrivals dominated by instantaneous changes in frequency. This may limit the performance of this picking algorithm, and it might be worthwhile to replace the STA/LTA detector with a more robust, but nevertheless fast picker like the Baer and Kradolfer picker or a picking algorithm based on higher order statistics. Furthermore, the implemented quality assessment in the Sleeman and van Eck version based on signal-to-noise ratio only is not sufficient for robust quality estimation of the derived P onsets. A more robust quality criterion might be the "sharpness" of the AIC function, as proposed by Diehl et al. (2009b). However, a multivariate improvement of the AR-AIC picker should also be able to pick precisely S-arrival times.

16.4 Automated S-onset determination

For robust location of earthquakes and especially for the determination of hypocentral dephts, the estimation of S-onset times is crucial (Gomberg et al., 1990). Furthermore, S-wave arrival times may be inverted for models of the S-wave velocity supplementing P-wave velocity models and yielding additional information e.g. for petrological interpretation and seismic hazard models. However, S phase picking is more difficult than P-phase picking due to the character of the later arriving shear wave. Although by far most of the seismic wave energy is contained in the S waves and accordingly their amplitudes are generally larger than those of the related P waves (see record examples of local, regional and teleseismic events in DS 11.1-11.3), the often weaker very initial S-wave onset is usually buried in the preceding P coda.

Statistical properties of the P coda are highly variable and usually not Gaussian distributed. Therefore, the S onset may not be detectable by algorithms based on higher order statistics. S waves show often emergent onsets and may be preceeded by S to P conversions. Moreover, while the energy of longitudinally polarized P waves is usually concentrated on the vertical component, the energy of the later arriving transversally polarized S waves is in general distributed over all three components. In addition, the occurence of S-wave splitting may complicate the determination of the S-wave arrival time (Fig. 16.16). Thus, even manual picking and phase identification is often uncertain and inconsistent and experience is needed to pick and identify reliably the S onset. Hence, automated S-phase arrival time estimation is a challenging task and the development of optimized automated algorithms for picking of arrival times of S phases or other later arriving phases is a topic of ongoing research and applications to large data sets are still rare.

Reliable automatic S-onset determination makes use of all components or at least of both horizontal components. Usually, automatic picking of later phases is an iterative process. First the P onset has to be determined using the vertical component, from which a time window for S-phase picking is derived. Alternatively, the S phase is picked in a time window predicted from a preliminary event location. Algorithms proposed for P phase picking may also be used for S-phase arrival time determination when applied to transversal components. For instance, the AR-AIC picker (Takanami and Kitagawa (1988, 1991), Sleeman and van Eck (1999), see sub-section 16.3.4), has the potential of picking later phases if applied to horizontal components. Leonard and Kennett (1999) investigated single- and multi-component autoregressive modeling techniques for P- as well as for S-onset time determination. For multi-component analysis, the AR coefficients are represented by a second-order tensor. The order of the autoregressive processes representing the noise and the signal parts of the seismogram, respectively, are obtained by fitting AR-power spectra to observed ones.

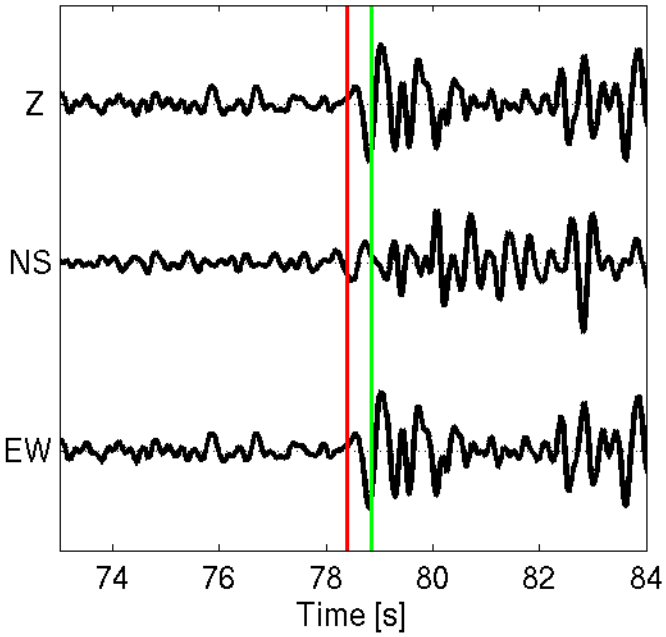

Fig. 16.16 Shear-wave splitting observed on a 2-10 Hz bandpass filtered local event recording. The green line indicates the SH-onset time, visible only on the north-south component. The red line indicates the SV-onset time, visible on the vertical and the east-west component.

Here, the algorithms proposed by Cichowicz (1993), Wang and Teng (1997) and Diehl et al. (2009b) are discussed in detail, as these algorithms are specifically developed for S-phase arrival time determination.

Cichowicz (1993) proposed an algorithm for automatic S-phase picking from three-component seismic data based on a polarization analysis, which is a powerful tool to distinguish between longitudinal and transversal energy, as discussed above. The algorithm might be described as follows:

Taking into account the dominating frequency, usually determined from displacement or velocity power spectrum, respectively, the length N of a moving window is determined. At first, the covariance matrix of the three orthogonal components of ground motion is computed within a window around the P onset, which is assumed to be known:

$$\begin{bmatrix} COV(X,X) & COV(X,Y) & COV(X,Z) \\ COV(Y,X) & COV(Y,Y) & COV(Y,Z) \\ COV(Z,X) & COV(Z,Y) & COV(Z,Z) \end{bmatrix} \tag{16.31}$$

where the estimate of the covariance for N observations of two variables X and Y is given by

$$COV(X,Y) = \frac{1}{N}\sum_{i}^{N}(x_i - \bar{x})(y_i - \bar{y}) \tag{16.32}$$

with $\bar{x}$ and $\bar{y}$ being average values. The direction of polarization is calculated by considering the eigenvector associated with the largest eigenvalue. Then, the X, Y and Z components are rotated into L, Q and T components, where L coincides with the principle direction of the P wave particle motion, i.e.

$$\begin{vmatrix} L \\ Q \\ T \end{vmatrix} = \begin{vmatrix} u_{11} & u_{12} & u_{13} \\ u_{21} & u_{22} & u_{23} \\ u_{31} & u_{32} & u_{33} \end{vmatrix} \cdot \begin{vmatrix} X \\ Y \\ Z \end{vmatrix} \tag{16.33}$$

where $u_{i,j}, j = 1,2,3$, are the direction cosines of the i-th principle direction. The covariance matrix and the following parameters are calculated for a moving window:
1) The deflection angle $F_1(t)$ - the angle between the current polarization and the P-wave polarization - given by

$$F_1(t) = \frac{cos^{-1}|u_{11}|}{\pi/2} \tag{16.34}$$

with u_{11} being the direction cosines in the L, Q, T coordinate system.
2) The degree of linear polarization $F_2(t)$

$$F_2(t) = \frac{(\nu_1 - \nu_2)^2 + (\nu_1 - \nu_3)^2 + (\nu_2 - \nu_3)^2}{2 \cdot (\nu_1 + \nu_2 + \nu_3)^2}, \tag{16.35}$$

with ν_1, ν_2, ν_3 being the eigenvalues of the covariance matrix at time t.

3) The ratio F_3 between transversal and total energy

$$F_3(t) = \frac{\sum_i^N (Q_i^2 + T_i^2)}{\sum_i^N (Q_i^2 + T_i^2 + L_i^2)} \tag{16.36}$$

These parameters are normalized and their theoretical values will be close to 1 for S waves. The CF is determined using these parameters:

$$CF(t) = F_1^2 \cdot F_2^2 \cdot F_3^2. \tag{16.37}$$

An S phase is declared, if the CF exceeds a threshold A for a few consecutive samples. A is calculated from the CF:

$$A = \overline{CF} + 3\sigma, \tag{16.38}$$

where $\overline{CF}$ is the average value of the CF and σ the variance of the CF in the time window. The uncertainty of the automatic S pick is not evaluated by this algorithm. Sleeman and van Eck (2003) combined the polarization analysis with wavelet tranform (Rioul and Vetterli, 1991) and applied their aproach to 313 local events. For their data, they found 44.1% to 47.9% of automatic S picks in the interval [-0.5, +0.5]s around the manual S onset and 65.5% to 68.9% of automatic S picks in the interval [-1.5, +1.5]s around the manual S pick.

Wang and Teng (1997) combine several approaches into an artificial neural network (ANN) algorithm. They consider the following properties of the three-component seismogram: (1) short-term to long-term average ratios (STA/LTA); (2) the ratios of transversal to total power (same as F_3 in Cichowicz, 1993); (3) the change of autoregressive model coefficients. As they assume a second-order AR process, this change becomes:

$$ARC(i) = \frac{|\, a_1(i)a_2(i) - a_1(i-1)a_2(i-1) \,|}{|\, a_1(i)a_2(i) \,|}, \tag{16.39}$$

where a_1, a_2 are the estimated AR coefficients.

(4) The fourth criterion is the deflection angle $D(t)$ or the short-axis incidence angle of the polarization ellipsoid, i.e.

$$D(t) = \frac{cos^{-1} |\, u_{31} \,|}{\pi/2}. \tag{16.40}$$

In their proposed ANN, each attribute is calculated by a neural subnet. The output of the subnets varies between 0 (no S phase) to 1. The output of the four subnets serve as input for the final decision unit, where the inputs are summed up. If the summation of inputs is larger than 3, the estimated arrival time is accepted.

Similar to their approach, Diehl et al. (2009b) propose a picking algorithm that combines STA/LTA ratios, polarization analysis, and AR-AIC picking (see sub-section 16.3.4). Combined STA/LTA ratios are calculated from both horizontal components as illustrated in Fig. 16.17. The picking algorithm is similar to the one proposed by Baer and Kradolfer (1987, see sub-section 16.3.2), but yielding an earliest (tS_{min1}) and latest (tS_{thr1}) possible pick, respectively.

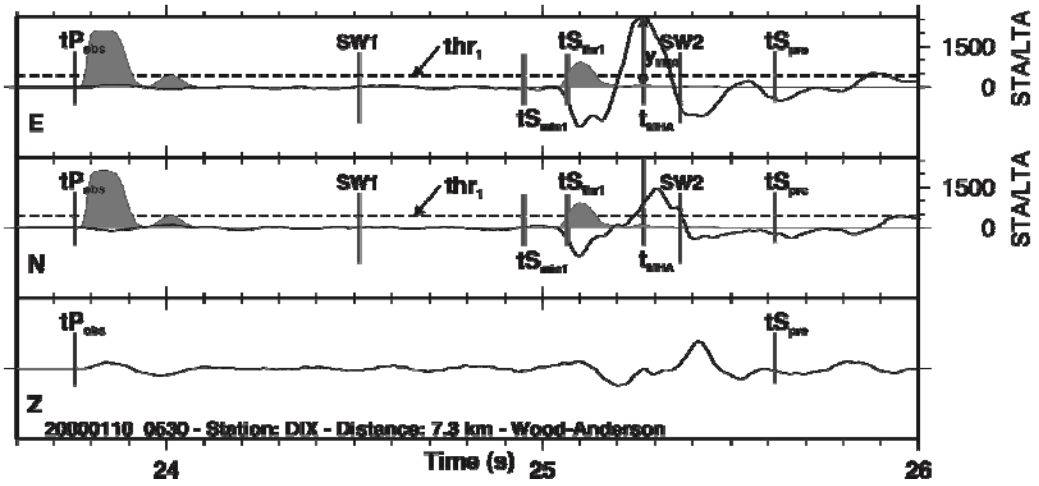

Fig. 16.17 Combined STA/LTA approach used for S-wave detection on horizontal components. Black solid curves represent the Wood-Anderson filtered three-component seismograms (amplitudes normalized by station maximum) of a local earthquake in Switzerland (Ml 3.1, focal depth of 9 km). The gray shaded trace denotes the combined STA/LTA ratio derived from N and E components. tP_{obs} represents the known P-arrival time, and tS_{pre} indicates the position of theoretical S arrival predicted from a regional one-dimensional model. The dashed horizontal line denotes the dynamic threshold thr_1 for the picking algorithm. The S-wave arrival time based on the STA/LTA detector in the potential S window (*SW1* to *SW2*) is most likely located in the interval between tS_{min1} (minimum pick) and tS_{thr1} (threshold pick). Copy of Fig. 2 in Diehl et al. (2009b, p. 1908) with © granted by the Seismological Society of America.

The polarization detector mainly follows the one proposed by Cichowicz (1993). In addition, they calculate a weighting factor $W(t)$ for each window, which accounts for the absolute amplitude within the centered window with respect to the maximum amplitude derived from the coarse S window, derived from the observed P onset and the theoretical S onset. The characteristic function CF of the polarization detector is:

$$CF(t) = F_1(t)^2 R(t)^2 F_3(t)^2 W(t), \tag{16.41}$$

with F_1 and F_3 being the deflection angle and the ratio between transversal and total energy, respectively, as introduced above. $R(t)$ is the rectilinearity:

$$R(t) = 1 - \frac{\nu_2 + \nu_3}{2 \cdot \nu_1}, \tag{16.42}$$

with ν_1, ν_2, ν_3 being again the eigenvalues of the covariance matrix. Fig. 16.18 illustrates the principle of the proposed polarization detector. A picking algorithm is applied to the derived CF, which yields an earliest (tS_{min2}) and latest (tS_{thr2}) possible estimate of the S phase arrival (see Fig. 16.18).

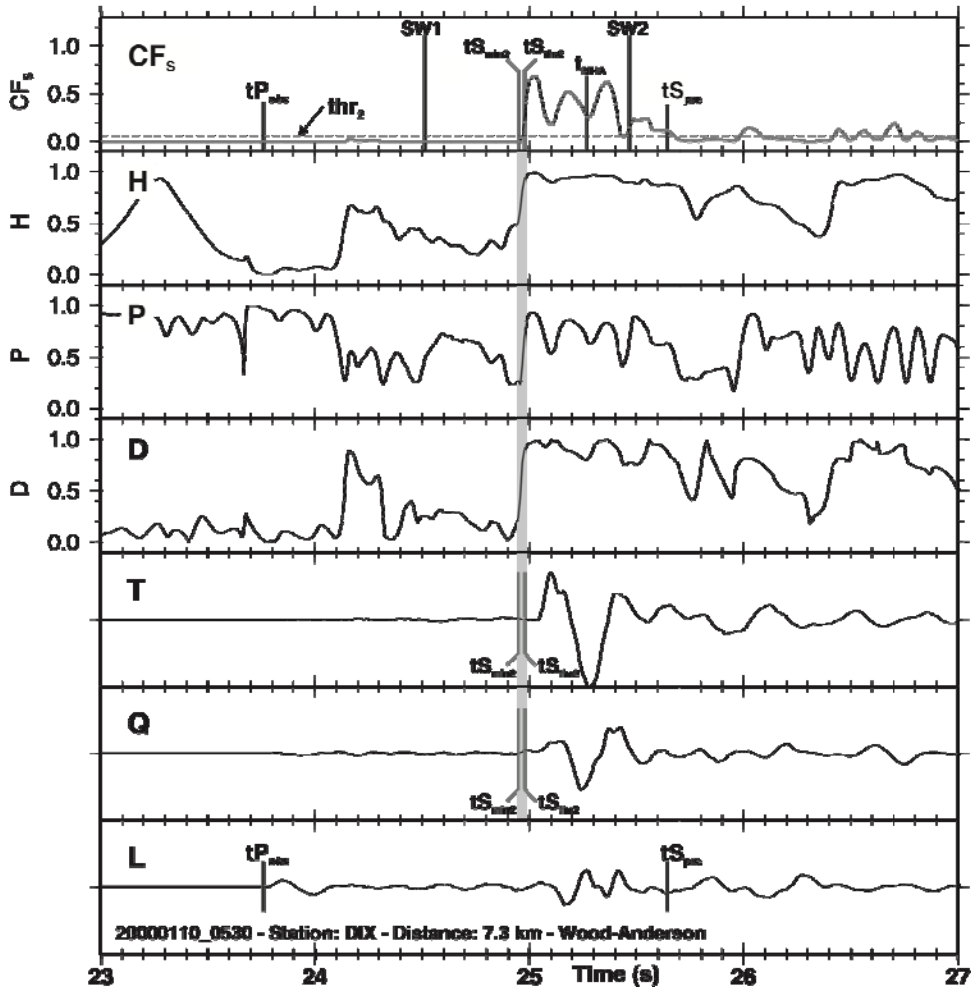

Fig. 16.18 Example for the polarization detector. L, Q, and T denote the rotated components. The corresponding S-wave operators are *D(t)* (directivity), *P(t)* (rectilinearity), and *H(t)* (transverse to total energy ratio). The uppermost trace represents the amplitude weighted characteristic S-wave function *CFS*. The arrival of the S wave (gray band) goes along with the simultaneous increase of *D(t)*, *P(t)*, *H(t)*, and *CFS*. Compared to the actual arrival on T, the S wave detection is shifted by approximately 0.1 sec to earlier times. This time shift is caused by the finite length of the polarization filter. *CFS* is not affected by the P wave. Copy of Fig. 3 in Diehl et al. (2009b, p. 1910) with © granted by the Seismological Society of America.

The information provided by the detectors is used to set up the search window for a AR-AIC picker, applied to single original and rotated components and to both horizontal components as illustrated in Fig. 16.19. The implementation is mainly based on the method of Takanami and Kitagawa (1988). Finally, the earliest and latest possible picks from the STA/LTA detector, polarization detector, and the different AIC minima are used to estimate the ultimate automatic S-wave arrival time and its corresponding uncertainty. Examples of final automatic S-phase picks of different uncertainty classes are shown in Fig. 16.20.

Diehl et al. (2009b) applied their proposed S-picking algorithm to 552 earthquakes in the Alps recorded at epicentral distances ≤150 km, resulting into an upper error bound of 0.27 seconds. Their data set is available at ORFEUS: http://www.orfeus-eu.org/Data-info/special_datasets.htm.

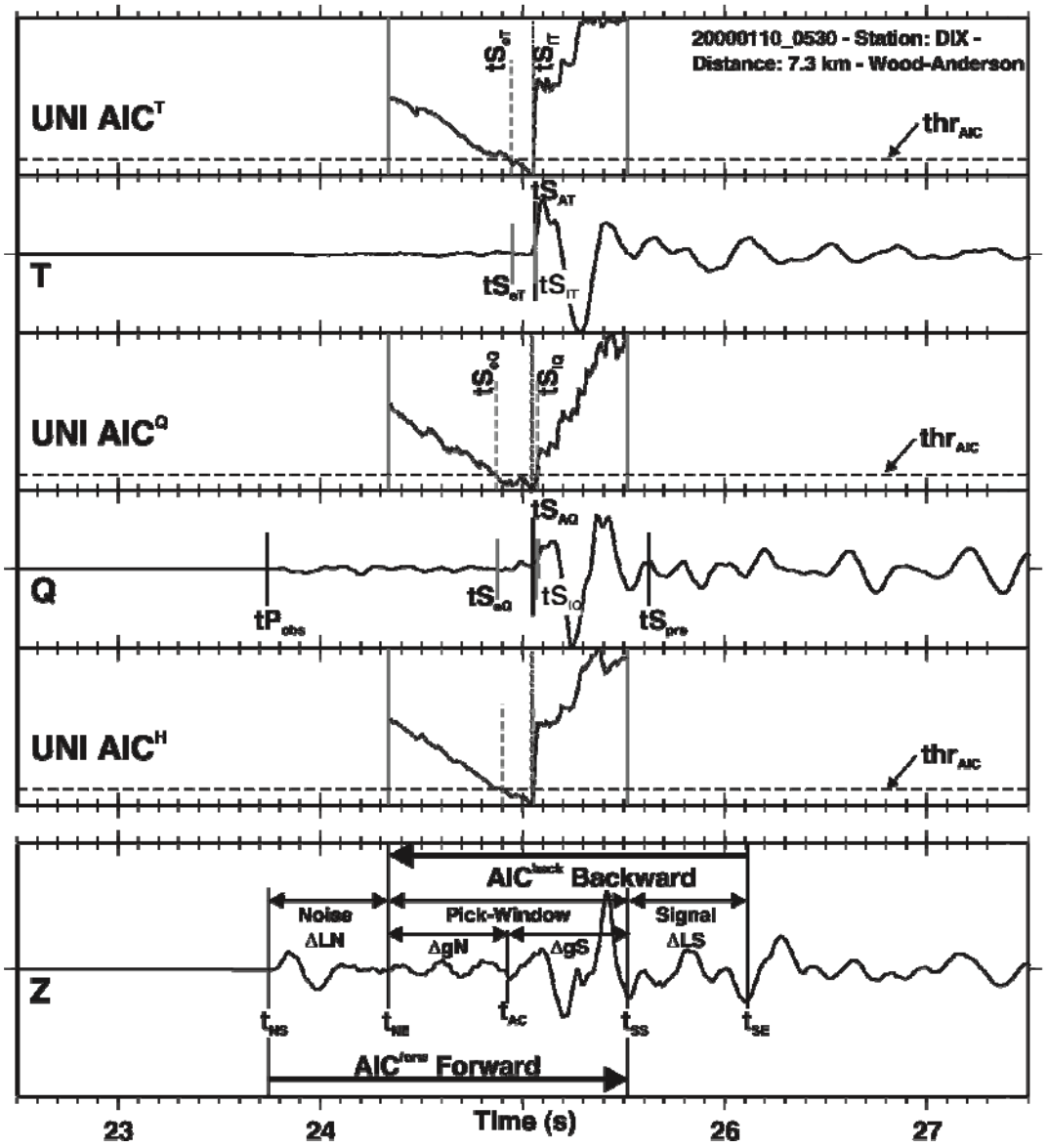

Fig. 16.19 Example of the AR-AIC picker. All amplitudes are trace normalized. The lower box illustrates the search window configuration centered around t_{AC}. The corresponding univariate AIC functions are shown for the combination of original E+N components (AIC^H) and for the rotated components Q (AIC^Q) and T (AIC^T). AR-AIC picks tS_{AQ} and tS_{AT} derived from the minimum on the AIC functions agree very well with the actual arrival of the S wave visible on the seismograms. The uncertainty of the AR-AIC pick is expressed by the earliest and latest possible arrival times tS_{eQ}, tS_{eT}, tS_{lQ}, and tS_{lT} derived from intersection of threshold thr_{AIC} (dashed horizontal lines) with the corresponding AIC functions. Copy of Fig. 4 in Diehl et al. (2009b, p. 1911) with © granted by the Seismological Society of America.

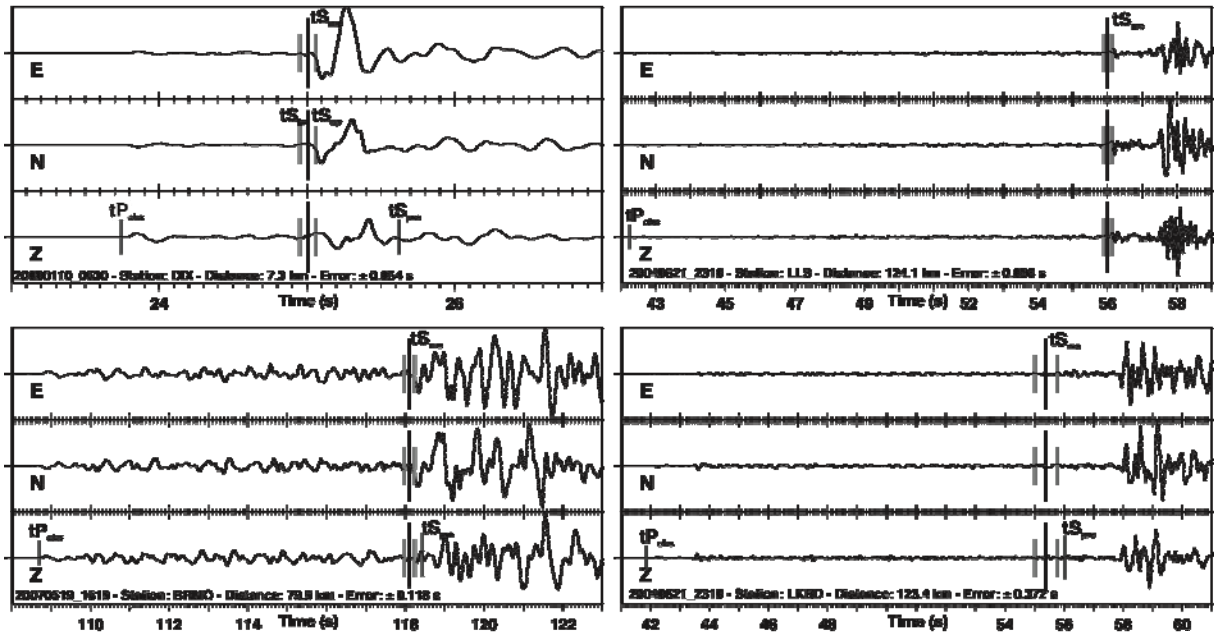

Fig. 16.20 Examples of automatic S-wave picks at epicentral distances dominated by first arriving Sg phases (left-hand column) and first arriving Sn phases (right-hand column) for different error intervals. The error interval derived from the automatic quality assessment is represented by the vertical gray bars. The vertical long black bars denote the mean position of the S-wave onset. Error interval and mean position agree very well with the actual S-wave arrival observed on the seismograms. Copy of Fig. 5 in Diehl et al. (2009b, p. 1914) with © granted by the Seismological Society of America.

16.5 Automated quality assessment, phase identification, and outlier detection

Resolution and reliability of travel-time based inversion techniques, like hypocenter determination and tomography, depend strongly on the consistency of data quality weighting. Arrival times with larger uncertainties have to be down weighted or even rejected in the inversion process. Uncertainties of arrival time picks are traditionally divided into discrete quality classes (e.g. 0 to 4, with 0 corresponding to highest quality and 4 corresponding to lowest quality). Each quality class is associated with a certain weight (between 1 and 0) and should correspond to a measured uncertainty interval (in seconds). Such discrete quality classification is still used in many location and tomography algorithms like HYPOINVERSE (Klein, 2002) or VELEST (Kissling, 1988), which convert the quality class to a data weight during inversion. Quantitative uncertainty measures are usually absent for arrival times in global bulletins. Instead, picks are simply classified as “impulsive”, “emergent”, or “questionable” based on wavelet characteristics. Such qualitative error assessment, however, no longer satisfies the resolution capability of modern digital waveform data.

Although often disregarded, the uncertainty of an arrival time pick consists of two components: uncertainty of the phase timing and uncertainty of the phase identification (e.g. Diehl et al. 2009b). Automated picking and association of later phases is challenging, but provides fundamental information on earth structure and hypocenter locations. Especially phases like PmP, S, pP, and sP are crucial to constrain focal depth of local and teleseimic earthquakes.

In this section, we discuss procedures for automatic quality assessment of phase timing and phase identification. Because automatic quality assessment sometimes overestimates the timing quality or misinterprets the phase, outlier picks have to be detected in post-picking procedures as described at the end of this section.

16.5.1 Quality assessment of phase timing

Arrival time estimation of phases needs to be accompanied by uncertainty estimates in order to down weight or even reject uncertain picks. The uncertainty of picks may be increased by low signal to noise ratios or by emergent onsets in contrast to impulsive ones. Emergent onsets are caused by the character of the source time function of the earthquake, the radiation pattern or by complicated wave propagation. Until now, only few papers focus on automatic quality assessment (e.g. Allen 1978; Aldersons 2004; Di Stefano et al. 2006; Diehl et al. 2009a and b; Nippress et al. 2010; Küperkoch et al. 2010) though automated arrival time determination should always be supplemented by automated uncertainty estimations.

Most widespread is the use of the signal-to-noise ratio (SNR) for automatic quality control and uncertainty estimation. Using certain window lengths depending on the dominating frequency, the amplitudes or the energy content right before the considered onset is compared to the amplitudes or energy content right after the onset (e.g. Sleeman and van Eck, 1999). If the SNR is calculated in the frequency domain, power spectral densities are compared (e.g. Leonard and Kennett, 1999). However, even bursts of noise may lead to large SNR, resulting in high qualities for false picks. To overcome this problem, it is necessary to estimate the signal length, which can be done by exploiting the envelope function (see Fig. 16.21) or by counting consecutive zero crossings of previous amplitudes, which exceed a certain threshold, as suggested e.g. by Allen (1978, see sub-section 16.3.1).

In addition to criteria for the SNR and the signal length, Allen (1978) uses a quite sophisticated algorithm for estimating the quality, based on analyses of the seismogram as well as of the CF (see sub-section 16.3.1). Küperkoch et al. (2010) suggest using the slope of the CF (sub-section 16.3.3) to identify emergent onsets. The MannekenPix algorithm of Aldersons (2004) includes a pattern recognition scheme, which weights nine different waveform attributes (predictors) obtained in the time window around the automatic pick and classifies the pick in discrete quality classes. The corresponding weighting factors are called “Fisher coefficients”, which have to be calibrated with a set of manually picked arrival times (reference picks).

A multiple discriminant analysis (MDA) is used to derive appropriate Fisher coefficients from the reference picks. Four predictors characterize the SNR. Predictor 5 is the difference between the dominant frequency of the signal and the dominant frequency of the noise. The remaining 4 predictors characterize properties of the CF around the estimated arrival time. This elaborated picking algorithm has been successfully applied to local earthquake data of the Dead Sea region (Aldersons, 2004), Italy (Di Stefano et al., 2006) and the greater Alpine region, respectively (Diehl et al., 2009a).

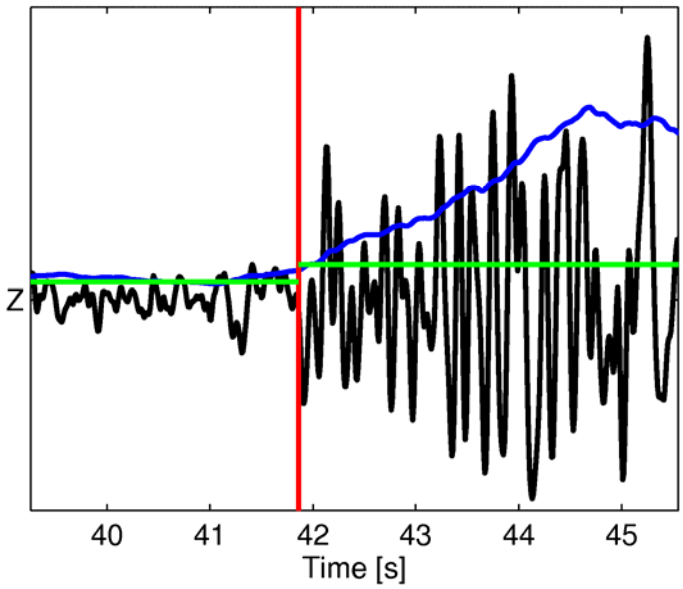

Fig. 16.21 Short-period seismogram, 2-10 Hz bandpass filtered (black), and corresponding envelope function (blue). The envelope function is used to confirm the automatically derived P onset. The noise level is calculated within a window (green horizontal line) right before the automatically derived P onset (red vertical line). For this regional waveform example the requirement is that at least 70% of the envelope within a window of 4 seconds should exceed the signal threshold (green vertical line after P onset), which is twice the noise level.

16.5.2 Phase identification

Automatically determined arrivals have to be identified, that means, phase names have to be assigned to the arrival times, indicating their fundamental type and path through the earth. Most automatic approaches are intended to pick the first arriving phase of either P or S branches. Therefore, any automatic pick is considered as first arriving phase. In practice, picking algorithms can miss the very first phase and misinterpret later phases or larger amplitudes in the coda as the first arrival. Such phase misidentification may result in errors in the arrival times of up to several seconds, as pointed out e.g. by Diehl et al. (2009a). Fig. 16.22 shows an example of a regional event recording, where Pn is picked by the analyst, while the automated procedure picked a more prominent later phase (likely PmP). In case of first-arrival studies, picks should be accompanied by first-order estimates on whether arrival time is associated with first or later arriving phase. So far, most algorithms do not include such uncertainty estimates of phase identification, however, the assessment of phase timing can be tuned to pick targeted phases as described e.g. by Diehl et al. (2009a).

Explicit phase association of arrival times is usually only possible in combination with *a priori* information on the Earth's structure and the location of the event. Phase identification, however, can be accomplished by an iterative procedure: a preliminary location is determined using first arriving P phases, then first (and later arrivals) are associated by comparison with theoretical arrival times. In addition, epicentral distances can be estimated from S-P times and polarization analysis may support the identification of later phases (see section 16.4).

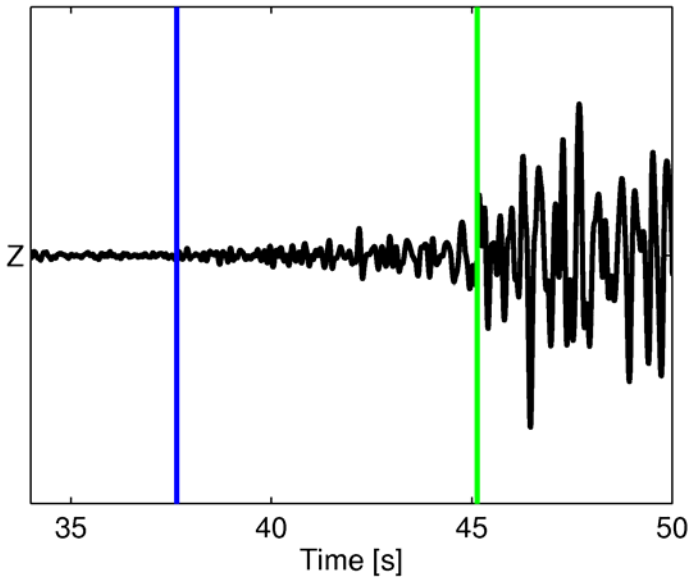

Fig. 16.22 Example of phase misidentification within a 2-10 Hz bandpass filtered record. First arriving Pn-phase (blue) and intermediate phase (likely Pg) is missed by the automatic approach using kurtosis. Instead, the automatic approach (green) picks a later phase (likely PmP). Such misidentification may result in errors of several seconds.

Recordings of local to regional earthquakes are dominated by crustal phases like Pg, Pn, and PmP. Later arrivals are often buried in the P and S coda and may occur within short time windows. In addition, the correct identification is challenging due to the heterogeneous structure of the crust, which leads to significant travel time residuals, attenuation, scattering, and interference of these phases. In general, identification of first and later arriving crustal phases requires good knowledge of the three-dimensional structure of the crust. On the other hand, teleseismic events are dominated by mantle and core phases (see Chapter 11) and, as discussed later, signal properties like amplitude ratios between components, polarization or slowness as well as travel time differences between phases may be used to identify phases in the record. Global one-dimensional travel time tables can be used to predict and associate arrival times with phases. Crucial later arriving phases like pP can be associated with probability models as e.g. implemented in the EHB (Engdahl, van der Hilst, Buland) relocation procedure of Engdahl et al. (1998).

In situ automatic identification of various phases of a seismic record requires detection algorithms sensitive to later arrivals. Earle and Shearer (1994) propose a detection algorithm based on STA/LTA ratios calculated from the envelope function using the Hilbert transform of the seismogram. In order to prevent rapid fluctuations in the ratio function, the ratio function is smoothed by convolution with a Hanning filter. They applied this algorithm to seven years of global data distributed by the National Earthquake Information Center (NEIC). A comparison with the ISC hand-picked phase arrival times encounters difficulties with phase arrivals characterized by a change in frequency and little or no change in amplitude. However, the proposed algorithm is a useful tool for extracting seismograms containing phases desired for further analysis, e.g. for phase association. Fig. 16.23 shows an application of the proposed algorithm to a regional event recording.

Tong and Kennett (1995) and Bai and Kennett (2000) developed an algorithm, which combines automated detection and phase association for first and later arrivals. The proposed procedures are rather sophisticated and it is beyond the scope of this manual to provide a detailed description. The algorithms include many components useful for development of future generations of automatic algorithms (e.g. data adaptive filtering, analysis of three-component records, pattern recognition, etc.) and therefore we summarize only the main features of their approaches here.

Tong and Kennett (1995) define a set of STA/LTA detectors that make use of all three components and compare STAs and LTAs from different components in order to detect later phases. They use an approach of continual updating (Tong, 1995), where the effective lengths of the STA and LTA windows are adapted to the dominating frequency. In addition, they propose optimized filters to enhance the possibility of later phase detections and detection on multiple frequency bands (see also sub-section 16.6.2). Ratios of the energy on the different components, the frequency content, as well as polarization properties are used to characterize and to identify detected phases. Three measures of the energy of the phases are introduced:

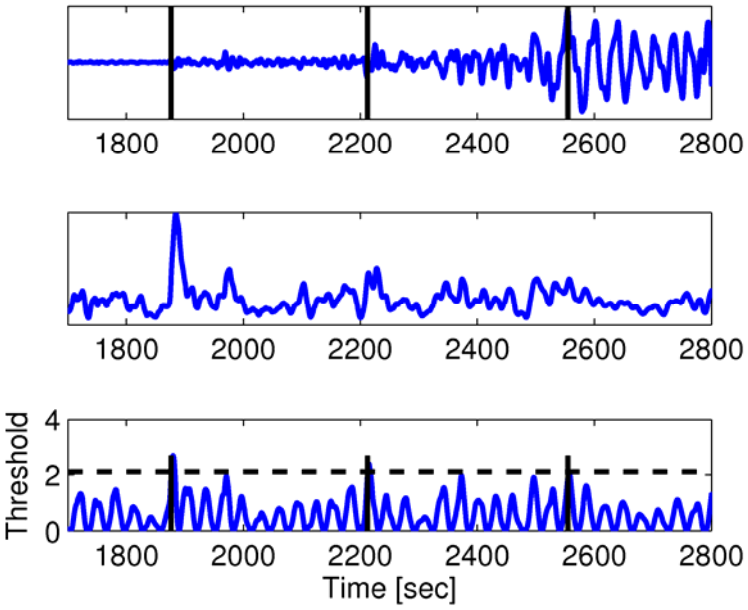

Fig. 16.23 Application of the proposed algorithm by Earle and Shearer (1994) for phase detection to a regional event recording at distance Δ = 3792 km (blue). Top: 0.01 – 0.1 Hz bandpass filtered waveform with recognized arrivals (vertical, black lines). Middle: corresponding STA/LTA ratios. Bottom: Smoothed ratio function (SRF, blue), applied threshold (dashed horizontal line) and detections (vertical black lines). This algorithm is useful for the detection of later arrivals rather than the precise arrival time determination.

1. the total energy $E_3 = Z^2 + N^2 + E^2$,
2. the vertical component energy $V_E = Z^2$,
3. the energy in the horizontal plane $H_E = N^2 + E^2$.

The LTA measure is calculated for the total energy E_3, while STA terms are calculated for the energy on each of the Z, N, and E components as well as for the horizontal energy H_E, and the

total energy E_3. This results in a set of five different STA/LTA triggers. The output of the STA/LTAs is used to detect as well as to identify phases. Tong and Kennett (1996) define a range of empirical conditions to identify the fundamental type of the detected phase as summarized in Tab. 16.4.

Tab. 16.4 Empirical conditions to identify the fundamental type of detected (later) phases proposed by Tong and Kennett (1996). Distance range far-regional to teleseismic is defined by slowness less than 0.12 km^{-1}.

P wave (far-regional to teleseismic)	SV-wave (far-regional to teleseismic)	P wave (regional)
$H_E < 0.50E_3$	$H_E > 0.50E_3$	$H_E > 0.50E_3$
$V_E > 0.35E_3$	$V_E < 0.35E_3$	$V_E > 0.35E_3$

Furthermore, simple indicators are introduced to characterize the waveform of the phases:

$$\widetilde{P} = V_E - 0.35E_3,$$
$$\widetilde{S} = H_E - 0.5E_3.$$

The set of five STA/LTA phase detectors is applied to the data adaptive high-pass (corner frequency: two times the dominant background noise frequency) as well as low-pass (corner frequency: half the dominant frequency background noise) filtered data.

Polarization properties of the phases are characterized in terms of azimuth and incidence angles of a "phase vector", which is constructed to describe the average behavior of the phase over a quarter cycle of the dominant period. Using these attributes Tong and Kennett (1996) developed a procedure for the identification of phases. It is assumed that the following six attributes are available for the each phase *i*:

1. t_i, the arrival time;
2. a_i, the amplitude;
3. ν_i, the local frequency;
4. ϕ_i, the azimuth in the horizontal plane;
5. ψ_i, the angle of incidence to the vertical;
6. c_i, the P or S type of the arrival.

An assumption tree is used for further identification (Tong and Kennett, 1996). In analogy to rules of thumb employed by expert seismologists a heuristic method is suggested. The phase identification follows the assumption tree given in Fig. 16.24, starting with key phases like P and S first arrivals. At each level of the assumption tree, a set of assumptions about a single factor is tested.

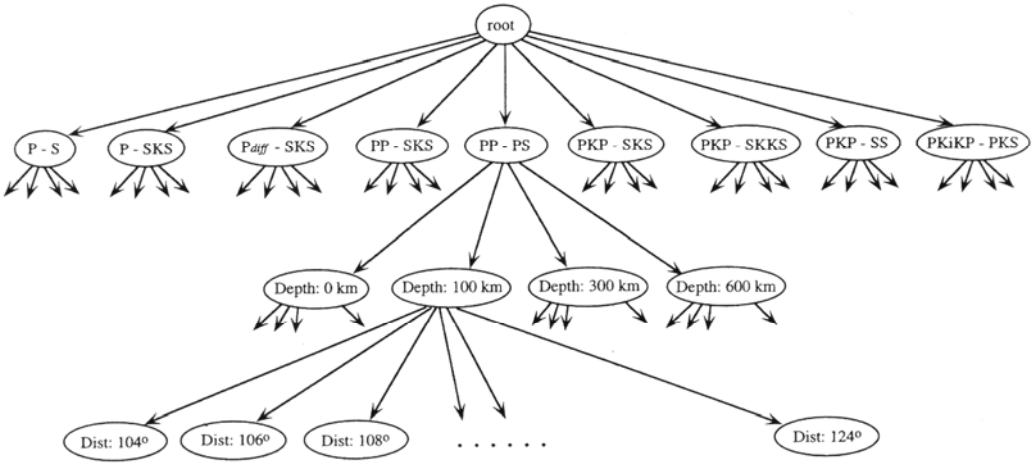

Fig. 16.24 Assumption tree for seismic event classification hierarchy (after Tong and Kennett, 1996).

At each node, the information of its parent node is gathered and includes extra information, starting with just the observed data. In case of contradictions, the branching associated with the current node is terminated. Otherwise the branching process continues with the evaluation of further hypothesis. When no further assumptions are to be tested, a solution is represented based on a set of hypothesis describing the data.

Tab. 16.5 Ranges of travel time differences between P and S phases for different epicentral distances for the heuristic method proposed by Tong and Kennett (1996).

P-S Identity	Time Interval Range [min]	Distance Range [^{0}]
P-S	2.18-10.43	12-85
P-SKS	9.37-10.65	82-99
P_{diff}-SKS	9.39-10.69	100-129
PP-SKS	3.96-7.22	82-129
PP-PS	9.20-10.14	104-125
PKP-SKS	5.84-7.21	114-143
PKP-SKKS	7.97-12.66	126-180
PKP-SS	20.05-27.66	136-180
PKIKP-PKS	3.35-3.60	126-141

16.5.3 Post-picking and outlier detection

As mentioned before, even the most sophisticated automated algorithms introduce, to some degree, erroneous picks. Phase misinterpretation as shown in Fig. 16.18 or overestimated pick uncertainties are usually inevitable. In the following, we present tools to detect outliers in post-picking procedures.

Most commonly, erroneous picks are identified by large residuals in the event location routine. Frequently applied location routines like HYPOINVERSE (Klein, 2002) or

HYPOSAT (Schweitzer, 2001) are able to exploit additional information like phase names, uncertainty estimates, and other phase properties such as polarization angles in order to identify inconsistent picks. Some of these routines automatically down weight observations associated with large residual. Although it is a common practice, we point out that the velocity model used for location biases residual weights. Therefore, residual weights from location routines should never replace the observation weights assigned by the picker. Otherwise, correct picks might be down weighted due to an insufficient velocity model and might be useless for tomographic studies.

Furthermore, the presence of few outlier picks can have a significant influence on the hypocenter solution derived by traditional least-square approaches. Beamforming techniques as described e.g. by Pinsky (2006) or the Equal Differential Time (EDT) formulation implemented in the NonLinLoc location routine of Lomax et al. (2000) yield very robust hypocenter solutions even in the presence of outliers and may therefore also improve the detection of false picks. In practice, automatic picks associated with large residual are usually flagged in the location routine and might be reviewed by the network analyst.

Identifying outliers in the location routine requires the presence of an appropriate velocity model of the study area. Since automatic pickers are increasingly used to derive such models, simultaneous inversion of hypocenters and seismic velocities have to be performed to detect outlier picks. Such iterative inversion procedures are proposed e.g. by Diehl et al. (2009a). Finally, Wadati diagrams as described, for example, by Kisslinger and Engdahl (1973) or Maurer and Kradolfer (1996) are used to identify mispicked S wave arrivals, independent of the P and S wave velocity structure.

16.6 Practical considerations: implementation, calibration, and pitfalls of automatic detection and picking procedures

Implementation and realization of automatic detection and picking procedures depend on the application purpose and the available data. Commonly, these automatic procedures are used in permanent seismic weak-motion networks to detect and locate events in real or near-real time and the focus is on low detection thresholds in order to generate earthquake catalogs as complete as possible. However, increasingly, such automatic procedures are nowadays also applied on records from very dense strong-motion accelerometer networks such as the Japanese K- and KiK nets (see Chapter 8, sub-section 8.7.3). They trigger events on higher detection thresholds. Therefore, these records are, as compared to very sensitive weak-motion records, less or not at all effected by the preceding microseismic noise. Nevertheless, sophisaticated algorithms are used to identify phase onset times. E.g. Akazawa (2004) uses a combination of STA/LTA ratios of a cumulative envelope function and the AR-AIC algorithm to exploit strong motion records of the K-, KiK-, and the CEORKA (Committee of Earthquake Observation and Research in the Kansai Area) networks. In any event, the calculated automatic locations have to be robust and available within minutes after an event. Finally, network applications have to handle signals in a broad frequency range in order to detect and pick events from local to teleseismic distances.

A second class of applications is the use within the increasing number of temporary deployments (aftershock deployments, temporary field deployments, etc.), which generate huge data volumes. Furthermore, the number of available analysts is usually limited. Focus for this class of applications is variable, but usually includes high detection rates for local to

regional events. Computing time of detection, picking, and location is less crucial and teleseimic events are already identified by global bulletins.

Finally, application of "re-picking" studies become increasingly important, in which automatic algorithms are used to improve consistency and quality of existing network picks, or to merge picks of several networks. For this class, event detection is usually not necessary and focus is on high-quality picks. Preliminary locations in combination with available earth models can be used to predict windows of first and later arriving phases. If arrival times are required for high-resolution tomography, consistency of picks is favored over hit-rate of algorithms, since completeness is less relevant. Numbers of erroneous picks, however, have to be as small as possible since residuals of outliers in the post-picking detection might be of the same order than residuals due to velocity anomalies. A suite of iterative detection stages might precede this "high-quality" application.

No matter which algorithm is chosen, automatic procedures have to be calibrated and tested with any new data set, i.e. the parameters of the algorithms have to be adjusted and optimized towards the application purpose. In this section we describe calibration and test procedures for automatic pickers. Furthermore, the pre-processing and quality of waveform data is crucial for reliable automatic procedures. Therefore, common pitfalls related to waveform filters and waveform quality are discussed at the end of this section.

16.6.1 Calibration and test of automatic pickers

Typically, calibration and test of automatic algorithms is achieved by comparison with a set of representative manually picked onset readings (e.g. Baer and Kradolfer 1987; Sleeman and van Eck 1999; Di Stefano et al. 2006). A common practice is the use of network picks (i.e. arrival times routinely picked by network analysts on a day-to-day basis) as reference for the automatic algorithms. These network picks, however, are usually not appropriate to serve as reference picks, because they yield a high level of noise due to mispicks and other inconsistencies, particularly in error assessment. Reference arrival times for calibration and meaningful tests of automatic algorithms have to be picked consistently. In addition, reference picks have to be provided with a consistent measure of uncertainty in terms of phase timing (see sub-section 16.5.1) and phase identification (see sub-section 16.5.2). Seismograms with no identifiable phases (e.g. due to low signal-to-noise ratio) have to be flagged, in order to test the automatic picker's ability to reject low-quality signals. Finally, consistent use of waveform filters during reference picking is necessary to avoid biases between automatic and manual picks. Additional use of theoretical arrival times, component rotation and tools like polarization analysis might be necessary for reliable reference picking of S waves. A detailed description on reference picking can be found in Diehl et al. (2009a) and IS 11.4. The set of reference picks should be divided in two subsets. The first subset is used to calibrate the algorithm and subsequently, the calibrated algorithm is tested with the other half.

Calibration of algorithms (i.e. adjustment of parameters) is usually accomplished by trial-and-error methods. Parameters are adjusted in order to minimize the difference between automatic and reference picks. As mentioned earlier, the trade-off between hit rate, precision, and number of outliers depends on the application purpose. Additional information on automatic quality assessment can be included in the performance evaluation using a matrix representation as suggested by Di Stefano et al. (2006). The quality assessment of the automatic picker must be tuned to get quality classes, which are similar or even equal to the

manually derived onset weights. Because automated algorithms usually evaluate the weighting classes differently than the analysts (e.g. using SNR determined from the seismogram and/or the CF, slope of CF, combination of both, etc.), the aim of exactly matching manual and automatic weighting classes is hard to achieve. In general, a sufficient calibration is obtained if the automatic picker upgrades only a very few low-quality reference picks to top quality classes and the majority of the high-quality reference picks is correctly classified as top quality. If only high-quality picks are requested (e.g. high-resolution tomography or high-precision relocation studies), the automatic quality assessment must be tuned such that none of the lowest-quality picks is classified as highest-quality (e.g. Di Stefano et al. 2006; Diehl et al. 2009a). As a consequence, a lot of intermediate-quality picks are rejected, resulting in an incomplete but high-quality set of arrival times. In contrast, for coarse location purposes the picker must be trained towards increased hit rate of intermediate-onset readings to assure a sufficient number of observations and azimuthal coverage for robust event location. Finally, to ensure that the calibrated algorithm is appropriate for the entire data set (and not just for the subset used for calibration), it should be tested with a second subset of reference picks as described earlier.

Sophisticated packages like MannekenPix (Aldersons 2004) or the algorithm proposed by Nippress et al. (2010) make use of data adaptive calibration in order to improve performance of picking and quality assessment and to avoid tedious trial-and-error procedures. Parameters are determined from the reference picks by an inverse technique based on pattern recognition. In practice, most automatic algorithms require a minimum of parameter search to determine the optimized choice of essential (data depending) picking parameters, such as search-window definitions or waveform filters.

16.6.2 Pre-processing: waveform filters

The estimation of arrival times depends on the chosen frequency band and differences in arrival times determined in different frequency ranges may be in the order of several seconds. The effect of waveform filters on the arrival time picking is illustrated in Fig. 16.25. On the other hand, application of filters often enhances the signal-to-noise ratio. High-pass filters are used to remove microseismic noise and low-pass filters are commonly used to eliminate anthropogenic noise. To minimize the bias introduced by inconsistent application of filters, only one frequency band should be used for picking. Filters should be of zero-phase-type to avoid systematic time shifts. For a consistent analysis of arrival times, filters used for reference picking should be identical with filters used during automatic picking.

In practice, however, the use of one fixed frequency band for picking is often inapplicable, especially when dealing with data of earthquakes from wide distance and magnitude ranges. Differences in frequency content of seismic signals are mainly caused by the source processes and to minor extend by phase shifts due to wave propagation (attenuation, finite frequency effects). Finite rupture processes of large earthquakes lead, especially in the near field, to very complex signals, dominated by low frequencies. Simpler signals are expected for the point-source characteristics of small and moderate magnitudes. Frequency content varies for local Pg, regional Pn, and teleseimic mantle or core phases and might even change with focal depth. Finally, the noise characteristic can be station dependant, especially for regional and global networks.

To account for the diversity in signal and noise characteristic, data adaptive filters like the Wiener filter can be used to enhance the signal-to-noise ratio of seismic data. The Wiener filter, as implemented in MannekenPix (Aldersons 2004), measures the power spectrum in two windows: $P_N(f)$ is determined from a window containing background noise and $P_{SN}(f)$ is measured in a window containing signal and noise. As described by Aldersons (2004) the Wiener filter can be approximated by:

$$W(f) \approx \frac{P_{SN}(f) - P_N(f)}{P_{SN}(f)}$$

The obvious advantage of the Wiener filter is that it affects only frequencies associated with the background noise. In the ideal case, the filter does not modify the signal part, in contrast to traditional high-, low-, or band-pass filters. This assumption, however, is only valid if the signal-spectrum does not overlap with the noise-spectrum. Implementations like in MannekenPix require *a priori* information on the approximate position of the onset (initial pick from predicted arrival time or some sort of preliminary pick) to properly setup the noise and signal+noise windows. A gap between both windows has to account for the uncertainty of the initial picks and the length of the windows have to be appropriate for the expected noise and signal frequencies. Improper choice of these parameters might introduce additional instabilities to the Wiener filter.

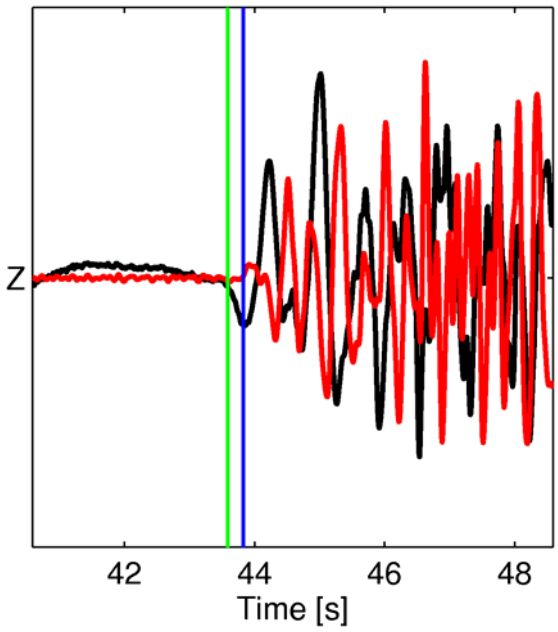

Fig. 16.25 Unfiltered (black) and filtered (red) local event waveform of a broadband record (Guralp CMG, 60 s – 50 Hz) using a 3rd order butterworth bandpass (2-10 Hz) and corresponding manual (blue vertical line) and automatic picks (green vertical line) indicating the effect of different filtering on P-onset determination. Note that in the more narrow-band high-frequency filtered record the amplitude of the first oscillations is strongly reduced, the negative first motion, still distinct in the broadband record, no longer recognizable and the phase of the oscillations significantly shifted. The reasons for these signal distortions due to filtering are discussed in Chapter 4.

A simple data adaptive filter is proposed by Tong (1995), who determines the dominant frequency f_n of the background noise and defines low- and high-pass filters based on f_n. Picking on multiple (fixed) frequency bands as well as filters depending on epicentral distance or station site might be used to account for differences in the signal and noise characteristics.

16.6.3 Pre-processing: waveform quality

The quality of available waveform data is crucial for reliable and robust automatic detection and picking procedures. "Glitches" present in time series can generate a high number of false picks and have to be identified and, if possible, removed prior to the picking. Common glitches are spikes, abrupt offsets in amplitudes (caused by data gaps or sensor re-centering), clipped amplitudes, and precursory oscillations prior to impulsive onsets (caused by instrumental acausal anti-alias filters). If filters are applied to these glitches and if they occur close to a seismic event, they are indistinguishable from real signals for most automatic algorithms. Spikes in the data can be identified and removed by running average routines as implemented e.g. in the SAC software. Clipped amplitudes usually inhibit reliable S wave detection and therefore, clipped seismograms have to be identified and removed prior to automatic S picking as described e.g. by Diehl et al. 2009b. Effects of acausal anti-alias filters can be removed by an inverse filtering process described e.g. in Scherbaum (2001) or may be minimized by application of certain low-pass filters. Problems with data quality are usually specific to networks and procedures to detect and remove them have to be developed and adjusted from case to case. Therefore, tests with reference data have to be used to identify these problems and to develop and calibrate tools to remove them.

Appendix

Some internet addresses providing source codes or binaries of some picking algorithms:

- Several seismological software and useful links:
http://www.orfeus-eu.org/Software/software.html
- MannekenPix (MPX):
http://faldersons.net/Software/MPX/MannekenPix.html
- S-picker by Diehl et al. (2009b):
http://www.ldeo.columbia.edu/~tdiehl/Data2Download/spicker1.3.4.publ.tar.gz

Acknowledgments

The authors would like to thank Peter Bormann, Joachim Saul, and Reinould Sleeman for carefull proof-reading and valuable suggestions.

References

Akaike, H. (1970). Statistical predictor estimation. *Ann. Inst. Statist. Math.*, **22**, 203-217.

Akaike, H. (1971). Autoregressive model fitting for control. *Ann. Inst. Statist. Math.*, **23**, 163-180.

Akaike, H. (1974). Markovian representation of stochastic process and its application to the analyses of autoregressive moving average processes. *Ann. Inst. Statist. Math.*, **26**, 363-387.

Akaike, H. (1974b). A new look at the statistical model identification. *IEEE Transactions on Automatic Control*,**19** (6), 716–723.

Akazawa, T. (2004). A technique for automatic detection of onset time of P- and S-phases in strong motion records, *13th World Conference on Earthquake Engeneering*, Vancouver, B.C., Canada, Paper No. 786.

Aldersons, F. (2004). Toward three-dimensional crustal structure of the Dead Sea region from local earthquake tomography. *PhD thesis*, Tel Aviv University, Israel.

Allen, R. V. (1978). Automatic earthquake recognition and timing from single traces. *Bull. Seism. Soc. Am.*, **68**, 1521-1532.

Allen, R. V. (1982). Automatic phase pickers: Their present and future prospects. *Bull. Seism. Soc. Am.*, **72**, 225-242.

Baer M., and Kradolfer U. (1987). An automatic phase picker for local and teleseismic events. *Bull. Seism. Soc. Am.*, **77**, 1437-1445.

Bai, Chao-ying, and Kennett, B. L. N. (2000). Automatic phase-detection and identification by full use of a single three-component broadband seismogram. *Bull. Seism. Soc. Am.*, **90**, 187-198.

Basseville, M., and Nikiforov, I. V. (1993). Detection of abrupt changes: Theory and application. *Prentice Hall Information and System Science Series, Prentice Hall*, Englewood Cliffs, New Jersey.

Box, G. E. P., Jenkins, G. M., and Reinsel, G. C. (1994). Time series analysis - Forecasting and control. *Prentice-Hall*.

Burg, J. P. (1975). Maximum entropy spectral analysis. *PhD thesis, Department of Geophysics, Stanford University*.

Cichowicz, A. (1993). An automatic S-phase picker, *Bull. Seism. Soc. Am*,. **83**, 1, 180-189.

Diehl, T., Kissling, E., Husen, S., Aldersons, F. (2009a). Consistent phase picking for regional tomography models: application to the greater Alpine region. *Geophys. J. Int.*, **176**, 542–554.

Diehl, T., Deichmann, N., Kissling, E. Husen, S., 2009b. Automatic S-wave picker for local earthquake tomography. *Bull. Seism. Soc. Am.*, **99**(3), 1906-1920.

Dietz, L. (2002). Notes on Configuring BINDER_EW: Earthworm's Phase Associator; http://www.isti2.com/ew/ovr/binder_setup.html.

Di Stefano, R., Aldersons, F., Kissling, E., Baccheschi, P., Chiarabba, C., Giardini, D. (2006). Automatic seismic phase picking and consistent observation error assessment: Application to the Italian seismicity. *Geophys. J. Int*., **165**, 121-134.

Douglas, A., Bowers, D., and Young, J. B. (1997). On the onset of P seismograms. *Geophys. J. Int.* **129**, 681–690.

Earle, P. S., and Shearer, P. M. (1994). Characterization of global seismograms using an automatic-picking algorithm. *Bull. Seism. Soc. Am.*, **84**, 366-376.

Engdahl, E. R., Van der Hilst, R. D., and Buland, R. P. (1998). Global teleseismic earthquake relocation with improved travel times and procedures for depth determination. *Bull. Seism. Soc. Am.*, 88, 722-743.

Freiberger, W. F. (1963). An approximation method in signal detection. Quart. *J. App. Math*. **20**, 373-378.

Gentili, S., and Bragato, P. (2006). A neural-tree-based system for automatic location of earthquakes in Northeastern Italy. *J. Seismology*, **10**, 73-89.

Gentili, S., and Michelini, A. (2006). Automatic picking of P and S phases using a neural tree. J. Seismology, **10**, 39-63.

Goforth, T., and Herrin, E. (1981). An automatic seismic signal detection algorithm based on the Walsh transform. *Bull. Seism. Soc. Am.*, **71**, 1351-1360.

Gomberg, J. S., Shedlock, K. M., and Roecker, W. W. (1990). The effect of S-wave arrival times on the accuracy of hypocenter estimation. *Bull. Seism. Soc. Am.*, **80**, 6, 1605-1628.

Groos, J. C., and Ritter, J. R. R. (2009). Time domain classification and quantification of seismic noise in an urban environment. Geophys. J. Int., accepted for publication.

Hartung, J. (1991). Statistik - Lehr- und Handbuch der angewandten Statistik. *Oldenbourg Publishing Company*, Vienna, Munich.

Hildyard, M. W., Nippres, S. E. J., and Rietbrock, A. (2008). Event detection and phase picking using a time-domain estimate of predominant period, T^{pd}. *Bull. Seism. Soc. Am.*, **98**(6), 3025-3032.

Hildyard, M. W., and Rietbrock, A. (2010). T^{pd}, a damped predominant period function with improvements for magnitude estimation. *Bull. Seism. Soc. Am.*, **100**(2), 684-698.

Johnson, C. E., Bittenbinder, A., Bogaert, B., Dietz, L., and Kohler, W. (1995). Earthworm: A Flexible Approach to Seismic Network Processing. *IRIS Newsletter*, **14**, 2, 1-4.

Joswig, M. (1987). Methoden zur automatischen Erfassung und Auswertung von Erdbeben in seismischen Netzen und ihre Realisierung beim Aufbau des lokalen 'Bochum University Germany'-Netzes. *Berichte des Instituts für Geophysik der Ruhr-Universität Bochum*, Reihe A, No. 23.

Kao, H., and Shan, S.-J. (2004). The source-scanning algorithm: mapping the distribution of seismic sources in time and space. *Geophys. J. Int.*, **157,** 589-594.

Kissling, E. (1988). Geotomography with local earthquake data. Rev. Geophys., **26**, 659-698.

Kisslinger, C., and Engdahl, E. R. (1973). The interpretation of the Wadati diagram with relaxed assumptions. *Bull. Seismol. Soc. Am.*, **63**, 1723-1736.

Kitagawa, G., Takanami, T, and Matsumoto, N. (2001).Signal extraction problems in seismology. *Int. Statist. Rev.*, **69**(1), 129-152.

Klein, F. (2002). User's Guide to HYPOINVERSE-2000, a Fortran program to solve for earthquake locations and magnitudes, *USGS, Open File Report* 02-171,123pp.

Klein, F. W. (2003). The HYPOINVERSE2000 earthquake location program. In: Lee, W. H. K., Kanamori, H., Jennings, P. C., and Kisslinger, C. (Eds.) (2003). International Handbook of Earthquake and Engineering Seismology, Part B. *Academic Press, Amsterdam*, 1619-1620.

Küperkoch, L., Meier, T., Friederich, W., and EGELADOS working group (2010). Automated P-wave arrival time determination using higher order statistics. *Geophys. J. Int.*, **181**(2), 1159-1170; doi: 110.111/j.1365-246X.2010.04570.x.

Lay, T., and Wallace, T. C. (1995). Modern global seismology. ISBN 0-12-732870-X, *Academic Press*, 521 pp.

Le Bras, R., Swanger, H., Sereno, T., Beall, G., Jenkins, R., Nagy, W., and Henson, A. (1994). Global association; Final Report. *Science Applications International Corporation Technical Report,* SAIC-94/1155.

Leonard, M. (2000). Comparison of manual and automatic onset time picking. *Bull. Seism. Soc. Am.*, **90**, 1384-1390.

Leonard, M., and Kennett, B. L. N. (1999). Multi-component autoregressive techniques for the analysis of seismograms. *Phys. Earth Planet Int.*, **113**, 247-263.

Lomax, A.,Virieux, J., Volant, P., and Berge, C. (2000). Probabilistic earthquake location in 3D and layered models: Introduction of a Metropolis-Gibbs method and comparison with linear locations. In: Thurberand, C. H., and Rabinowitz, N. (2000). Advances in Seismic Event Location. *Kluwer, Amsterdam*, 101-134.

Longbottom, J., Walden, A. T., and White, R. E. (1988). Principles and application of maximum kurtosis phase estimation. *Geophysical Prospecting*, **36**, 115-138.

Maeda, N. (1985). A method for reading and checking phase times in autoprocessing system of seismic data. *Zisin=Jihin* (*J. Seism. Soc. Japan*), **38**,365-379.

Maurer, H., and Kradolfer, U. (1996). Hypocentral parameters and velocity estimation in the western Swiss Alps by simultaneous inversion of P- and S-wave data. *Bull. Seismol. Soc. Am.*, **86**, 32-42.

Michael, A. J., Gildea, S. P., and Pulli Jay, J. (1982). A real-time digital seismic event detection and recording system for network applications. *Bull. Seism. Soc. Am.*, **72**, 6, 2339-2348.

Morita, Y., and Hamaguchi, H. (1984). Automatic detection of onset time of seismic waves and its confidence interval using the autoregressive model fitting. *Zisin*, **37**, 281-293.

Nippress, S. E. J., Rietbrock, A., and Heath, A. E., (2010). Optimized automatic pickers: application to ANCORP data set. *Geophys. J. Int.*, **181**, 911-925.

Pinsky, V. (2006). Using beamforming for the global network location. *Phys. Earth Planet Int.,* **158**, 75-83.

Rawlinson, N., and Kennett, B. L. N. (2004). Rapid estimation of relative and absolute delay times across network by adaptive stacking. *Geophys. J. Int.***, 157**, 332-340.

Rioul, O., and Vetterli, M. (1991). Wavelets and signal processing. *IEEE Signal Proc. Magazine*, October 1991, 14-38.

Rowe, C. A., Aster, R. C., Borchers, B., and Young, C. J. (2002). An automatic, adaptive algorithm for refining phase picks in large seismic data sets. *Bull. Seism. Soc. Am.*, **92**, 5, 1660-1674.

Saragiotis, C. D., Hadjileontiadis, L .J.,and Panas, S. M. (2002). PAI-S/K: A robust automatic seismic P phase arrival identification scheme. *IEEE Trans. Geosci. Remote Sensing***, 40**, 1395-1404.

Scherbaum, F. (2001). Of poles and zeros: Fundamentals of digital seismology. Modern Approaches in Geophysics, *Kluwer Academic Publishers*, 2nd edition, 265 pp. (including an CD-ROM by Schmidtke, E., and Scherbaum, F. with examples written in Java).

Scherbaum, F., and Johnson, J. (1992). Programmable Interactive Toolbox for Seismological Analysis (PITSA). IASPEI Software Library Volume 5, Seismological Society of America, El Cerrito.

Schweitzer, J. (2001). HYPOSAT – An enhanced routine to locate seismic events. *Pure and Appl. Geophys.*, **158**, 277-289.

Sleeman, R., and van Eck, T. (1999). Robust automatic P-phase picking: an on-line implementation in the analysis of broadband seismogram recordings. *Phys. Earth Planet. Int.*, **113**, 265--275.

Sleeman, R., and van Eck, T. (2002). Single station real-time P and S phase pickers for seismic observatories. In: Methods and applications of signal processing in seismic network operations. Takanami, T. and Kitagawa, G. (Eds.). Springer-Verlag, Berlin, 173-194.

Stewart, S. W. (1977). Real-time detection and location of local seismic events in Central California. *Bull. Seism. Soc. Am.,* **67**, 2, 433-452.

Takanami, T., and Kitagawa, G. (1988). A new efficient procedure for estimation of onset times of seismic waves. *J. Phys. Earth*, **36**, 267-290.

Takanami, T., and Kitagawa, G. (1991). Estimation of the arrival times of seismic waves by multivariate time series model. *Ann. Inst. Stat. Math.,* **43**, 407--433.

Tong, C. (1995). Characterization of seismic phases - an automated analyser for seismograms. *Geophys. J. Int.,* **123**, 937-947.

Tong, C., and Kennett, B. L. N. (1995). Towards the identification of later seismic phases. *Geophys. J. Int.,* **123**, 948-958.

Tong, C., and Kennett, B. L. N. (1996). Automatic seismic event recognition and later phase identification for broadband seismograms. *Bull. Seism. Soc. Am.,* **86**, 6, 1896-1909.

VanDecar, and Crosson, R. S. (1990). Determination of teleseismic relative phase arrival times using multi-channel cross-correlation and least squares. *Bull. Seism. Soc. Am.*, **80**, No. 1, 150-169.

Wang, J, and Teng, T. (1997). Identification and picking of S phase using an artificial neural network. *Bull. Seism. Soc. Am.*, **87**(5), 1140-1149.

Withers, M. M., Aster, R. C., and Young, Ch. (1998). An automated local and regional seismic event detection and location system using waveform correlation. *Bull. Seism. Soc. Am.*, **88**, No. 3, 657-669.

Zeiler, C., and Velasco, A. A. (2009). Seismogram picking error from analyst review (SPEAR): single-analyst and institution analysis. *Bull. Seism. Soc. Am.*, **99**, 5, 2759-2770.

Zhang, H., Thurber C., and Rowe C. (2003). Automatic P-wave arrival detection and picking with multiscale wavelet analysis for single-component recordings. *Bull. Seism. Soc. Am.*, **93**, 1904-1912.